Available online at www.sciencedirect.com
SCIENCE DIRECT®
Geochimica et Cosmochimica Acta 70 (2006) 3883–3904
Geochimica
www.elsevier.com/locate/gca

Sr isotopes and pore fluid chemistry in carbonate sediment of the Ontong Java Plateau: Calcite recrystallization rates and evidence for a rapid rise in seawater Mg over the last 10 million years

Matthew S. Fantle [a,*,1], Donald J. DePaolo [a,b]

[a] Department of Earth and Planetary Science, University of California, Berkeley, CA 94720-4767, USA
[b] Earth Sciences Division, Lawrence Berkeley National Laboratory, Berkeley, CA 94720, USA

Received 13 January 2006; accepted in revised form 6 June 2006

Abstract

The $^{87}Sr/^{86}Sr$ ratios and Sr concentrations in sediment and pore fluids are used to evaluate the rates of calcite recrystallization at ODP Site 807A on the Ontong Java Plateau, an 800-meter thick section of carbonate ooze and chalk. A numerical model is used to evaluate the pore fluid chemistry and Sr isotopes in an accumulating section. The deduced calcite recrystallization rate is 2% per million years (%/Myr) near the top of the section and decreases systematically in older parts of the section such that the rate is close to 0.1/age (in years). The deduced recrystallization rates have important implications for the interpretation of Ca and Mg concentration profiles in the pore fluids. The effect of calcite recrystallization on pore fluid chemistry is described by the reaction length, L, which varies by element, and depends on the concentration in pore fluid and solid. When L is small compared to the thickness of the sedimentary section, the pore fluid concentration is controlled by equilibrium or steady-state exchange with the solid phase, except within a distance L of the sediment–water interface. When L is large relative to the thickness of sediment, the pore fluid concentration is mostly controlled by the boundary conditions and diffusion. The values of L for Ca, Sr, and Mg are of order 15, 150, and 1500 meters, respectively. L_{Sr} is derived from isotopic data and modeling, and allows us to infer the values of L_{Ca} and L_{Mg}. The small value for L_{Ca} indicates that pore fluid Ca concentrations, which gradually increase down section, must be equilibrium values that are maintained by solution-precipitation exchange with calcite and do not reflect Ca sources within or below the sediment column. The pore fluid Ca measurements and measured alkalinity allow us to calculate the *in situ* pH in the pore fluids, which decreases from 7.6 near the sediment–water interface to 7.1 ± 0.1 at 400–800 mbsf. While the calculated pH values are in agreement with some of the values measured during ODP Leg 130, most of the measurements are artifacts. The large value for L_{Mg} indicates that the pore fluid Mg concentrations at 807A are not controlled by calcite-fluid equilibrium but instead are determined by the changing Mg concentration of seawater during deposition, modified by aqueous diffusion in the pore fluids. We use the pore fluid Mg concentration profile at Site 807A to retrieve a global record for seawater Mg over the past 35 Myr, which shows that seawater Mg has increased rapidly over the past 10 Myr, rather than gradually over the past 60 Myr. This observation suggests that the Cenozoic rise in seawater Mg is controlled by continental weathering inputs rather than by exchange with oceanic crust. The relationship determined between reaction rate and age in silicates and carbonates is strikingly similar, which suggests that reaction affinity is not the primary determinant of silicate dissolution rates in nature.

1. Introduction

Deep-sea sediments represent a rich natural laboratory for the study of low-temperature geochemical processes. The sediments and associated pore fluids have accumulated slowly on the ocean floor over millions of years. Chemical interactions such as dissolution and precipitation of primary

* Corresponding author. Fax: +1 814 863 7823.
E-mail address: msf17@psu.edu (M.S. Fantle).
[1] Present address: Geosciences Department, Pennsylvania State University, University Park, PA 16802, USA.

0016-7037/$ - see front matter © 2006 Elsevier Inc. All rights reserved.
doi:10.1016/j.gca.2006.06.009

and secondary minerals are reflected in the chemical and isotopic composition of the pore fluids. In many sections there is negligible fluid flow, so the only transport in the fluid phase is by aqueous diffusion. The Deep Sea Drilling Project (DSDP) and subsequent programs have systematically sampled the sediments by coring long continuous sections and separating and archiving pore fluids. This paper is the first of a two part series aimed at using the pore fluids from a particular section of carbonate ooze and chalk—Site 807A on the Ontong Java Plateau—to better understand the Sr and Ca isotope geochemistry of marine carbonates and re-evaluate the implications of concentration gradients of Ca and Mg in the pore fluids.

Recent work on the calcium isotope evolution of Cenozoic seawater (De La Rocha and DePaolo, 2000; Schmitt et al., 2001; DePaolo, 2004; Fantle and DePaolo, 2005), as well as laboratory studies (Gussone et al., 2003; Lemarchand et al., 2004), have raised questions about the Ca isotope fractionation factor between dissolved Ca^{2+} and calcite. Laboratory experiments, in which calcite is precipitated from oversaturated solutions on a timescale of hours, produce calcite with isotopically fractionated Ca relative to Ca^{2+} in solution. Whether this fractionation is an equilibrium or kinetic isotope effect is not agreed upon (DePaolo, 2004). Deep-sea carbonate sediments and their associated pore fluids, which have been in contact for many millions of years, present an opportunity to determine the equilibrium fractionation factors for calcite in a natural system where the rates of exchange are several orders of magnitude slower, and the timescale of the experiment several orders of magnitude longer, than the laboratory experiments. In the case of deep-sea carbonate sediments, the first question that arises is whether equilibrium should be expected in associated pore fluids. If equilibrium is attained in these systems, which elements are at equilibrium and how does one demonstrate it? The current study seeks to use Sr isotopes and other pore fluid measurements to evaluate the extent to which the pore fluid Sr, Mg, and Ca geochemistry of the Site 807A marine carbonate section can be understood in terms of models for chemical and isotopic equilibrium, exchange, and transport.

We present Sr isotopic data on bulk carbonate and pore fluids from Site 807A and use the data to estimate the rate at which calcite is dissolving and precipitating. This approach is an extension of previous work (Richter and DePaolo, 1987, 1988; Richter, 1993, 1996; Richter and Liang, 1993) aimed at estimating rates of carbonate recrystallization in deep-sea sediments from Sr isotopic measurements. Site 807 has not previously been investigated for this purpose, but is a particularly good subject for study because the sediments sampled extend back in age to ~35 Ma, are relatively pure calcite, and represent nearly continuous sedimentation. Using new high-precision Sr isotopic measurements of sampled pore fluids (rather than distilled water rinses of the sediment of some previous studies), we can place tighter constraints on recrystallization rates. The results confirm that the recrystallization rates are low but significant, and decrease with sediment age up to at least 30 Ma. We use the derived recrystallization rates to evaluate the degree to which the pore fluid is in equilibrium with calcite for Ca and Mg, and then assess the significance of the gradients in pore fluid dissolved Ca and Mg concentrations. We show that the calcite recrystallization rates are sufficiently high so that the pore fluid Ca concentrations must represent equilibrium values everywhere below 30 mbsf and hence do not reflect deep sources of Ca^{2+}. In contrast, the pore fluid Mg concentrations are not in equilibrium with coexisting calcite and are only slightly affected by calcite recrystallization. Instead, we argue that pore fluid Mg concentrations at Site 807A constitute a unique record of Late Cenozoic paleo-seawater Mg concentration.

2. Sample location and description

Site 807 (ODP Leg 130) is located on the northern rim of the Ontong Java Plateau (3°36.42′N, 156°37.49′E; Fig. 1a), and sits in a shallow basement graben at 2804 meters water depth (Kroenke et al., 1991b). Drilling at Hole A reached a depth of 822.90 mbsf (meters below seafloor) and recovered core composed of nannofossil ooze to nannofossil chalk with variable foraminifer content and minor silicates (Fig. 1b). The carbonate section is deposited on 113–117 Ma oceanic crust with a thickness of 40 km. The $CaCO_3$ content of the sediment at 807A averages about 92%. Based on nannofossil biostratigraphy, the record at 807A spans the Quaternary, Neogene, and Oligocene. While Site 807A does not reach basement, drilling at nearby Site 807C (<60 meters away) indicates that the depth to basement at Site 807 is near 1380 mbsf so that there is an additional 550 meters of sediment below the deepest cored sediment at Site 807A.

Age assignments are made using a linear fit to the biostratigraphic control points identified by Kroenke et al. (1991b) (Fig. 2a). The oldest sediments cored at 807A are early Oligocene (33.5 Ma). We assume based on evidence from Site 807C that sedimentation at the site began around 76 Ma. At 33.5 Ma, the sedimentation rate (uncorrected for compaction) was 37 m/Myr (Kroenke et al., 1991b). This high sedimentation rate is followed by a 2 Myr hiatus during the late-early Oligocene (30.2–28.2 Ma) and then a return to 30 m/Myr during the late Oligocene to early Miocene. The sedimentation rate varied between 15 and 44 m/Myr during the Neogene (Fig. 2b).

3. Analytical methods

The procedures for the chemical separation and mass spectrometric analysis of Sr are similar to those described by Capo and DePaolo (1990). Because of the relative purity of the carbonate samples, and the fact that calcium carbonate can be preferentially dissolved when mixed with silicates, deep-sea carbonate ooze with small amounts of silicate can be analyzed with minimal chemical preparation

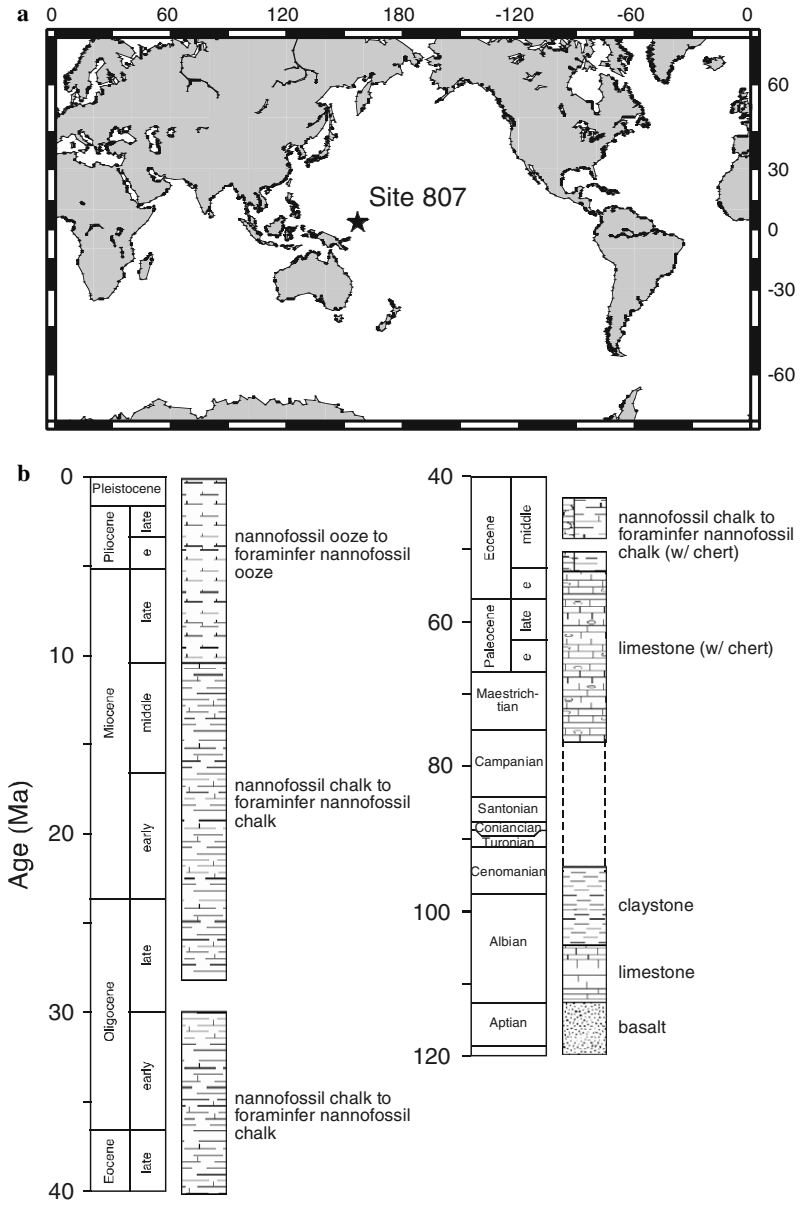

Fig. 1. (a) Location map and (b) composite stratigraphic column for ODP Site 807. Drilling at 807A (3°36.42′N, 156°37.49′E) reached ~823 mbsf while drilling at nearby 807C (3°36.39′N, 156°37.48′E) reached a total depth of ~1528 mbsf (1380 mbsf is the transition from sediment to basalt). Stratigraphic column after Berger et al. (1991).

and, hence, minimal sample contamination. Samples are dissolved in acetic acid and centrifuged. After extracting the supernatant, aliquots are taken for the determination of (1) Sr, K, and Rb concentration by isotope dilution and (2) Sr isotopic composition ($^{87}Sr/^{86}Sr$).

Weighed aliquots of acetic acid soluble carbonate are spiked with a mixed tracer containing ^{41}K, ^{87}Rb, and ^{84}Sr. After equilibrating the sample and the tracer, the spiked samples are loaded onto Re filaments and analyzed on a VG Sector 54 single-collector thermal ionization mass spectrometer for the concentrations of K, Rb, and Sr. For isotopic analysis, Sr is separated using Sr Spec resin (Eichrom resin: see Maher et al., 2003). The ion exchange columns used are acid-washed Teflon, with a column volume of 250–300 μl and a reservoir volume of 750 μl. The frit is made from a porous polyethylene sheet, with a pore size <90 μm. The Sr Spec resin is slurried with water and the fine particles decanted. About 250 μl of resin is added to the column and alternately rinsed six times with full column volumes of 4–6 N HCl and deionized water. The resin is then conditioned with 0.5 ml of 3 N HNO_3 and the sample added in 3 N HNO_3. The sample is rinsed with about 1 ml of 3 N HNO_3 and the Sr collected in 5 full column volumes of water. Because of the selective nature of Sr Spec resin and the possibility of cross contamination, the resin is discarded after one use. Strontium blanks for the column procedure are 0.5–1 ng for each 10–100 μg Sr sample (<0.01%) and Sr yields are between 90 and 95%.

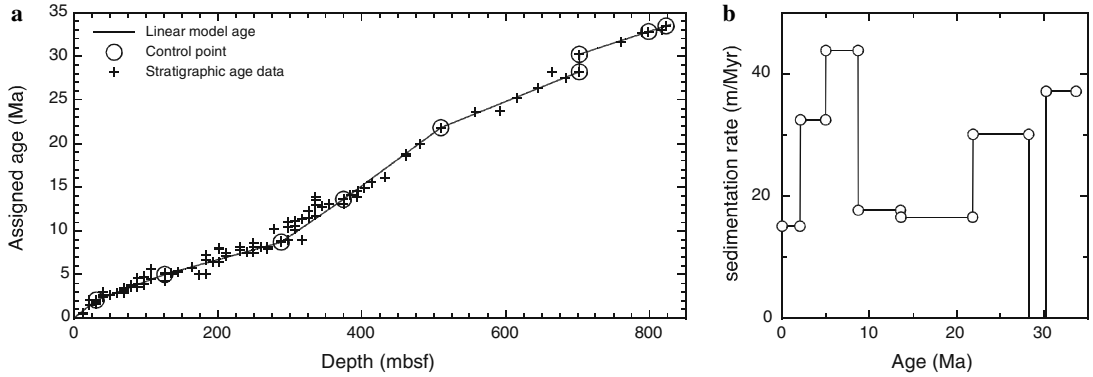

Fig. 2. (a) Age model for Site 807A, in which the biostratigraphic control points (○) identified by Kroenke et al. (1991b) are fit with a piecewise linear function. (b) Sedimentation rates (m/Myr) at 807A (○) determined using the piecewise linear depth-age model. The sedimentation rates are uncorrected for compaction.

Following ion exchange separation, 100 ng of dissolved Sr (in a solution of 1% H_3PO_4) are loaded with TaCl onto a single Re filament. Samples are measured on a Finnigan Triton multicollector thermal ionization mass spectrometer in static mode, with standard internal errors <0.0007%. The $^{88}Sr^{+}$ beam intensity is between 4 and 10 V during analysis, which utilizes a rotating amplifier procedure and collects data over 100–200 scans. Peaks are monitored at ^{88}Sr, ^{87}Sr, ^{86}Sr, ^{85}Rb, and ^{84}Sr. Repeated measurements of the Sr isotope standard NBS-987 on the Triton over a 12-month period yield a $^{87}Sr/^{86}Sr = 0.710241 \pm 0.000011$ (2 sigma of the distribution). Seawater measured on the Triton at Berkeley has a $^{87}Sr/^{86}Sr$ value of 0.709175.

4. Results: chemical and isotopic data from site 807A

Chemical and isotopic data measured in this study are shown in Tables 1 and 2, and in Figs. 3f–g. The pore fluid chemical data shown in Figs. 3a–e and h–j are from Kroenke et al. (1991b). Porosity decreases from about 0.7 to about 0.5 through the 800 meter section while temperature increases from 4 to 11 °C. The Site 807 pore fluids have typical depth profiles of Ca, Mg, Sr, and SO_4^{2-} concentrations. The measured pH values are bimodal and, as discussed below, the higher values are most likely affected by exchange with atmospheric CO_2 prior to onboard measurement of pH. The Sr concentrations in the acetic acid soluble fraction of the carbonates are similar to other deep-sea carbonates (Richter and Liang, 1993), with an average of about 17 ± 1 mmolal. The pore fluid Sr profile, which is similar to profiles at DSDP Sites 289, 590B, and 593 (Richter and Liang, 1993), reaches a maximum of about 930 μM Sr at 195 mbsf and remains relatively constant (875 ± 14 μM) in the deeper pore fluid samples with a slight trend toward lower values with depth.

The Sr isotopic compositions of the acetic acid soluble carbonate fraction, which we take to be representative of the bulk carbonate, vary from 0.709171 (4.45 mbsf) to 0.707946 (794.4 mbsf). The measured values are close to those inferred for seawater although there are slight shifts due to diagenesis. As discussed further below, the diagenetic shift of $^{87}Sr/^{86}Sr$ in the Site 807 carbonates is smaller than for the other sites (590B and 575) where there are detailed Sr isotope data (Richter and DePaolo, 1988). The important feature of the $^{87}Sr/^{86}Sr$-depth curve (Fig. 3g) is the kink centered around 400 mbsf, which gives the solid profile a shape similar to a sine curve superimposed on a linear decrease of $^{87}Sr/^{86}Sr$ with depth. The pore fluid $^{87}Sr/^{86}Sr$-depth curve generally tracks the solid curve, but with a much less pronounced "kink". The smoothness of

Table 1
Chemical data for pore fluids from ODP Site 807A

Sample[a]	Depth[b] (mbsf)	[K][c] (mM)	[Rb][c](μM)	[Sr][c] (μM)	$^{87}Sr/^{86}Sr$[d]
1H-3 145–150	4.45	10.80	1.67	130	0.709116
9H-4 145–150	79.85	11.40	1.66	619	0.708969
18H-4 145–150	165.35	10.88	1.62	904	0.708909
36X-3 140–150	335.30	10.54	1.46	899	0.708754
45X-5 140–150	425.70	10.44	1.45	876	0.708622
54X-4 0–10	509.60	10.21	1.38	878	0.708469
72X-2 140–150	681.10	9.85	1.36	862	0.708200

[a] Sample names are indicated by Core-Section Interval. Interval indivated in cm.
[b] Depth in meters below seafloor (mbsf).
[c] Concentrations as reported in Kroenke et al. (1991b). Errors at 2σ level are: K (±6%), Rb (±4%), Sr (±4%) (Kroenke et al., 1991a).
[d] Relative to seawater value of 0.709175. Errors at 2σ level are ⩽0.00001.

Table 2
Chemical data for marine carbonates from ODP Site 807A

Sample[a]	Depth[b] (mbsf)	Biozone[c]	Age[d] (Ma)	[K][e] (mmolal)	[Rb][e](μmolal)	[Sr][e] (mmolal)	$^{87}Sr/^{86}Sr$[f]
1H-1 95–86	0.95	NN20	0.06	15.8	8.4	19.8	0.709171
1H-4 14–15	4.64	NN20	0.31	17.3	4.7	18.0	0.709151
3H-2 15–16	18.55	NN19	1.23	12.7	—	15.5	0.709105
9H-4 33–34	78.73	NN13–NN14	3.54	7.4	14.0	19.9	0.709044
12H-2 107–108	104.97	NN12	4.35	9.8	3.9	19.8	0.709033
18H-4 74–75	164.64	NN11	5.88	11.4	3.4	17.2	0.708956
18H-5 74–75	166.14	NN11	5.91	11.8	2.9	18.0	0.708960
23H-2 109–110	209.49	NN11	6.90	6.0	2.0	17.1	0.708936
36H-3 107–108	334.97	NN8–NN6	11.36	17.3	4.1	16.6	0.708839
42X-2 102–103	391.72	NN5	14.64	9.3	8.4	16.3	0.708802
45X-5 57–58	424.87	NN5	16.65	—	—	12.2	0.708752
45X-6 65–66	426.45	NN5	16.74	10.7	4.1	13.6	0.708735
54X-3 114–115	509.24	NN2	21.76	7.1	1.3	16.6	0.708406
63X-4 59–60	596.69	NN2–NN1	24.69	9.1	2.7	16.7	0.708235
72X-2 66–67	680.36	NP24	27.47	8.7	2.5	17.9	0.708070
72X-3 78–79	681.98	NP24	27.52	9.6	3.0	17.3	0.708062
75X-2 86–87	709.56	NP23	30.39	6.8	1.8	17.9	0.708028
84X-1 48–49	794.38	NP23	32.68	5.5	1.6	16.1	0.707946

[a] Sample names are indicated by Core-Section Interval. Interval indivated in cm.
[b] Depth in meters below seafloor (mbsf).
[c] Nannofossil biozones as reported in Kroenke et al. (1991b).
[d] Based on piecewise linear fit to biostratigraphic control points (Kroenke et al., 1991b). See Section 2.
[e] As measured by isotope dilution thermal ionization mass spectrometry (mmol or μmol/kg carbonate). Errors at the 2σ level: K (±2%), Rb (±2%), Sr (±1.5%).
[f] Relative to seawater value of 0.709175. Errors at 2σ level are $\leqslant 0.00001$.

the pore fluid Sr isotope profile relative to the solid isotope profile is the key feature that provides information about calcite recrystallization rates in the section.

5. Estimating recrystallization rates

In this section, we use the pore fluid and solid Sr isotope ratios and concentrations to estimate the recrystallization rates of the Site 807A carbonate sediments. There are four processes that affect the Sr isotope ratio of pore fluids. The first process is dissolution-reprecipitation of the solid calcite. While dissolution contributes Sr to the pore fluids that has the isotopic composition of the solids, reprecipitation forms solid that has the same isotope ratio as the pore fluid dissolved Sr. If dissolution-precipitation were the sole or dominant process, then the pore fluids and the solids would have exactly the same isotope ratio at all depths, because the solid contains about 20 times more Sr than the pore fluid. However there is a second process, diffusion of aqueous Sr in the pore fluid, that competes with dissolution-precipitation. Diffusion acts to homogenize pore fluid concentrations and isotope ratios throughout the sediment column. The ocean supplies the upper boundary condition for the system. Since the ocean is a large reservoir of dissolved Sr, diffusion in the absence of dissolution-precipitation would create pore fluids with Sr isotopic composition equal to seawater. The complication is that the seawater isotope ratio has been increasing with time over the past 35 million years (DePaolo and Ingram, 1985), in a manner that is exactly the same as the change in solid $^{87}Sr/^{86}Sr$ with age. The third process is the weathering of basalt underlying the sedimentary section. The basalt of the Ontong Java Plateau has $^{87}Sr/^{86}Sr$ values of about 0.7034–0.7044 (Mahoney et al., 1993), much lower than the carbonate (0.709171–0.707946) and modern seawater (0.709175) values. Dissolution of minerals from the basalt produces pore fluid with low $^{87}Sr/^{86}Sr$; this basalt-derived pore fluid can then mix by diffusion with the pore fluid in the sedimentary section. Any basalt weathering flux should significantly lower the pore fluid $^{87}Sr/^{86}Sr$ values near the basalt–sediment interface. For the Site 807A carbonates that we are concerned with here, the basalt–sediment interface is about 550 meters below the base of the sampled carbonate section (at a depth of ~1350 mbsf at nearby Site 807C) and should not significantly affect the pore fluid Sr isotopes in the upper 800 meters of the section. The fourth process under consideration is the deep circulation of modern seawater into and through the sediment section (Baker et al., 1991; Richter, 1993), which would shift the pore fluid Sr concentrations to lower values and the $^{87}Sr/^{86}Sr$ ratios to higher values. Lateral flow into the sediment section usually occurs near the basalt–sediment interface, and counteracts the effects of basalt weathering. The sites where there is evidence for deep seawater circulation (e.g., DSDP Sites 572–575) are on normal oceanic crust in tectonically active terrain (the Clipperton Fracture Zone in the cases of Sites 572–575: Baker et al., 1991). There is no evidence of a significant flux of modern seawater into the sedimentary section at Site 807, which overlies the relatively stable Ontong Java Plateau.

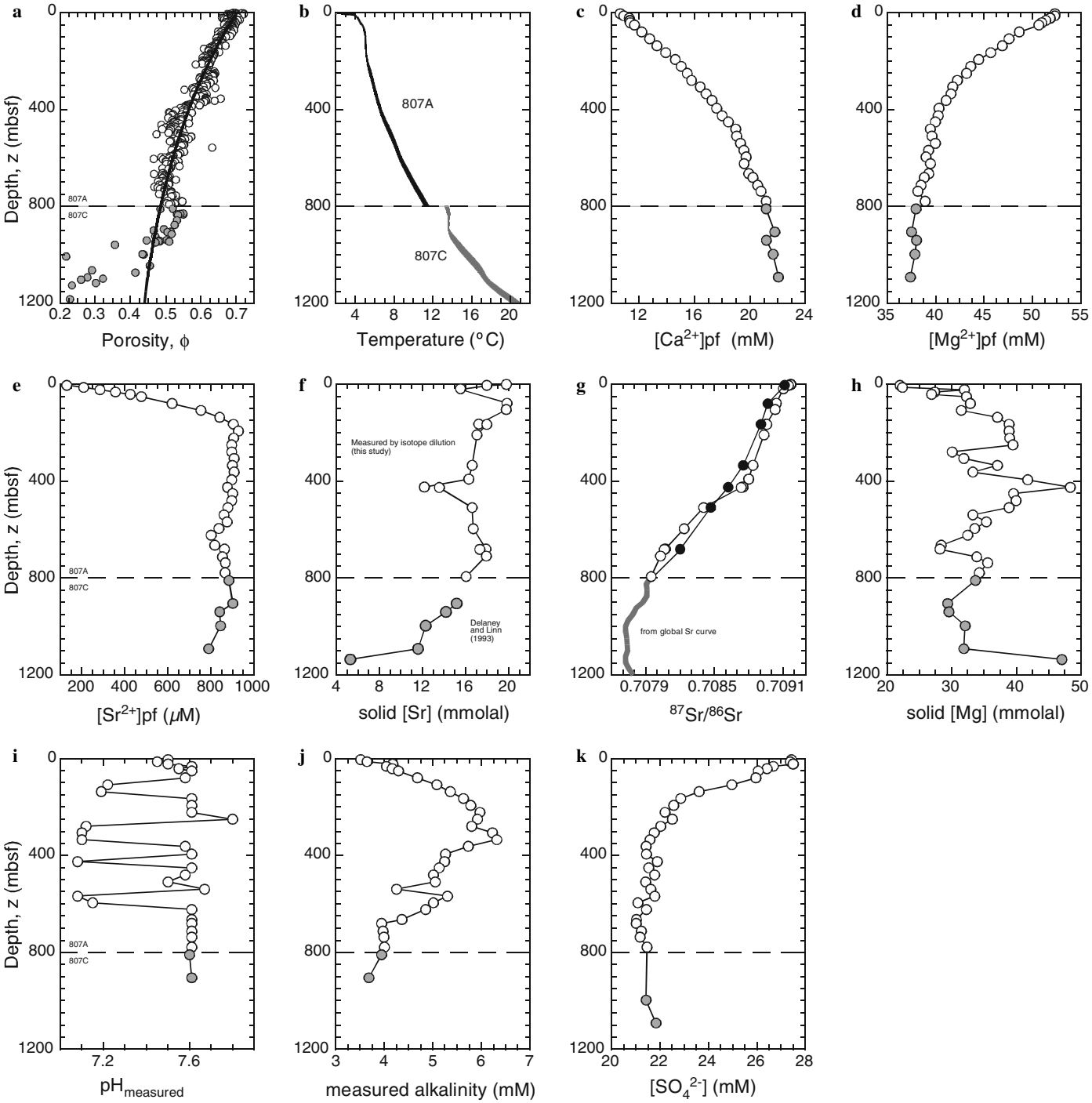

Fig. 3. Summary of geochemical and physical parameters at Sites 807A (0–800 mbsf) and 807C (800–1200 mbsf): (a) measured porosity (○) and exponential curve fit, (b) measured *in situ* temperature (°C), (c) pore fluid Ca concentration (mM), (d) pore fluid Mg concentration (mM), (e) pore fluid Sr concentration (μM), (f) carbonate Sr concentration (mmole Sr/kg acetic acid soluble carbonate), (g) $^{87}Sr/^{86}Sr$ of pore fluids (●) and acetic acid soluble carbonate (○), (h) carbonate Mg concentration (mmol Mg/kg carbonate), (i) measured pH (“free” pH scale), (j) total alkalinity (mM), and (k) pore fluid SO_4^{2-} concentration (mM). The curve fit for porosity is of the form $a + be^{(-z/c)}$, where $a = 0.37120 \pm 0.02521$, $b = 0.330793 \pm 0.02384$, and $c = 753.13235 \pm 88.94025$. The data shown in panels (a–e) and (h–j) are from Kroenke et al. (1991b). The original data in panels (f) and (g) are indicated by ○, while previously reported data for Site 807C are indicated by gray circles in (f). The portion of the global Sr curve used in the model is shown by the gray line in (g).

5.1. Reactive mass transfer equations

The approach used for the determination of recrystallization rates is similar to that described by Berner (1980), developed for use in carbonate sediments by Richter and DePaolo (1987), and subsequently used in a number of other studies (Richter and DePaolo, 1988; Richter, 1993, 1996; Richter and Liang, 1993; Schrag et al., 1995;

Rudnicki et al., 2001a,b). As discussed in detail by Richter and DePaolo (1987) and subsequent authors, the evolution of the concentration (C_f) of an element dissolved in the pore fluid can be described adequately by the equation:

$$\frac{\partial C_f}{\partial t} = D\frac{\partial^2 C_f}{\partial z^2} - v\frac{\partial C_f}{\partial z} + RM(C_s - KC_f) \quad (1)$$

for a system consisting of a monomineralic solid that is dissolving and reprecipitating such that there is no net change in the solid mass with time. In Eq. (1), D is the diffusion coefficient of the species in the aqueous phase, v is the advection velocity, C_s is the concentration in the solid, R is the rate at which the solid is recrystallizing (in units of reciprocal time), M ($=\rho_s(1-\phi)/\rho_f(\phi)$) is the local solid/fluid mass ratio, and K is the equilibrium distribution coefficient of the element between the solid and the fluid (C_s/C_f at equilibrium). The one-dimensional spatial reference frame is defined with $z = 0$ at the basalt–sediment interface, where z is positive in the upwards direction. Thus, an advection velocity (v) that is directed upwards has a positive sign while that directed downwards (towards the basalt–sediment interface) has a negative sign. In our defined reference frame, fluid movement is due only to advection and compaction-induced flow.

The evolution of the solid component is described by:

$$\frac{\partial C_s}{\partial t} = -V\frac{\partial C_s}{\partial z} - R(C_s - KC_f) \quad (2)$$

In the case of marine sediments, V is the compaction velocity. Solid-state diffusion is assumed to be negligible, so that the solid and fluid exchange only by dissolution and precipitation of the solid. In the reference frame we have defined, the solid does not move so that the term V refers only to compaction. Eq. (2) can be simplified by assuming that compaction is negligible (Richter, 1993).

5.2. Steady-state estimates of recrystallization rates

The best approach to estimating recrystallization rates in deep sea sediment sections is to use a numerical model to take into account diffusion, advection, and reaction over the timescale of interest. While we do this in the next section, we feel it is useful at this point to assess the qualitative effects of recrystallization, by deriving approximate values for recrystallization rates using a steady-state solution ($dC_f/dt = 0$) to the equations above. The initial and boundary conditions used are those that apply to a deep-sea carbonate section. We then assume that (1) the solid does not change concentration with depth or time (C_s = constant), (2) the fluid concentration at the upper boundary is fixed at the modern seawater concentration, (3) the porosity, distribution coefficient (K), and recrystallization rate (R) are constant with depth and time, and that there is no compaction ($V = 0$). Under these conditions, the steady-state solution to Eq. (1) is:

$$C_f(z) = \frac{C_s}{K} + \left(C_{sw} - \frac{C_s}{K}\right)e^{-z/L} \quad (3)$$

and the exponential factor is:

$$L^{-1} = \left(\frac{v^2}{4D^2} + \frac{RMK}{D}\right)^{1/2} - \frac{v}{2D} \quad (4)$$

For the limiting case in which $v = 0$, the length scale L becomes the diffusive reaction length (Berner, 1980; Phillips, 1991; DePaolo and Getty, 1996). Specifically, the diffusive reaction length for Sr (L_{Sr}) is:

$$L_{Sr} = \left(\frac{D_{Sr}}{RMK_{Sr}}\right)^{1/2} \quad (5)$$

The Sr reaction length determines the depth range over which the Sr concentration of the pore fluids changes from the seawater value (about 90 μM) to the equilibrium value (about 910 μM).

From the Sr data at 807A, we estimate L_{Sr} to be about 90 meters. Using $M = 1.1$ ($\phi = 0.7$), $D_{Sr} = 7500$ m^2/Myr, and $K_{Sr} = 20$ (see discussion below) we calculate $R = 0.042$ Myr^{-1}. This value for R applies to the upper 100–200 meters of the sedimentary section. Inclusion of upward advection would lower the estimate of R. For an upward advective flux of 15 m/Myr, the estimate of R decreases by ~20% to 0.034 Myr^{-1}.

For the deeper part of the section, we recognize that the diffusive reaction length Eq. (5) also describes the relationship between the fluid-phase Sr isotopic ratio and the solid-phase Sr isotopic ratio as a function of depth. For a fluid–solid system undergoing steady-state exchange, DePaolo and Getty (1996) showed, in the case of uniform fluid concentration, that if the solid isotopic ratio-depth profile is described by a Fourier series:

$$r_s(z) = A_0 + Bz + \sum_{n=1}^{\infty} A_n \sin\frac{2n\pi z}{\lambda} \quad (6)$$

then the steady-state fluid-phase isotopic ratio (r_f) is:

$$r_f(z) = A_0 + Bz + \sum_{n=1}^{\infty} a_n A_n \sin\frac{2n\pi z}{\lambda} \quad (7)$$

and the coefficients (a_n) are a function of the reaction length, L:

$$a_n = \frac{(\lambda/2n\pi L)^2}{1 + (\lambda/2n\pi L)^2} \quad (8)$$

Since steady-state diffusion produces a linear isotopic ratio profile when the Sr concentration is invariant (which it is to a good approximation), we detrend the Sr isotope data for the pore fluids and solids (Fig. 4c, for example). The detrended solid isotope data look roughly like a sine curve with a wavelength of $\lambda_{Sr} \approx 900$ meters and a peak-to-peak amplitude of ~0.0003. The detrended pore fluid isotope data also resemble a sine curve with the same wavelength and phase as the solid, and a peak-to peak amplitude of ~0.0001. Using equation 19 of DePaolo and Getty (1996), the reaction length can be calculated from:

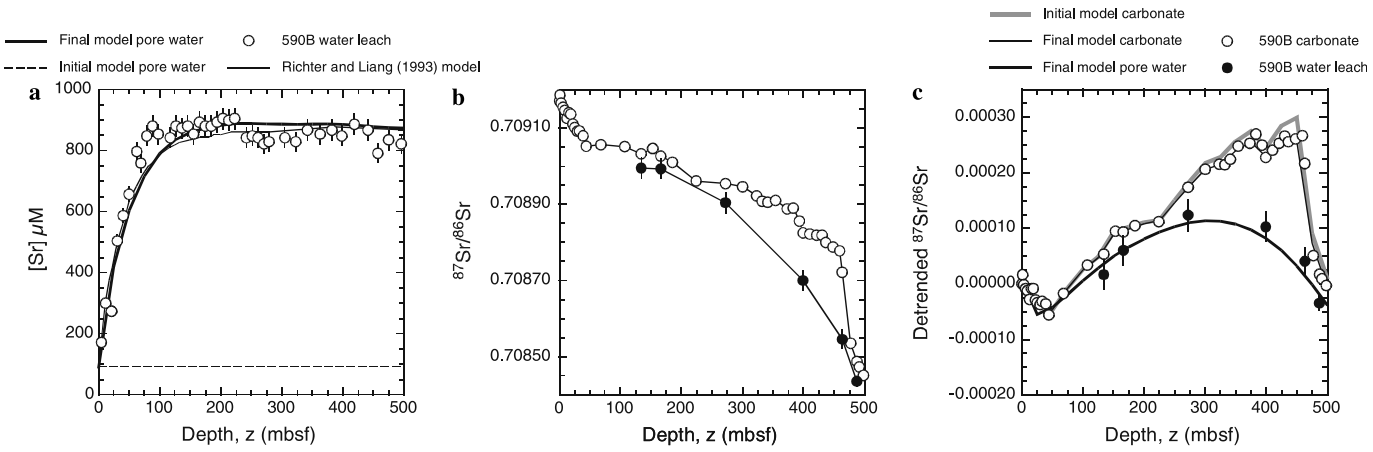

Fig. 4. Strontium model results and data for 590B pore fluids using the depositional diffusion-reaction model and the "reaction rate-age" relationship derived by Richter and Liang (1993). (a) The results of the depositional model applied to DSDP Site 590B pore fluid Sr concentrations (μM), (b) the Sr isotope data for 590B carbonates and associated water leaches (DePaolo, 1986), and (c) the results of the model applied to pore fluid $^{87}Sr/^{86}Sr$. The model pore fluids are illustrated with the bold lines in (a) and (c). The initial $^{87}Sr/^{86}Sr$ of the solid phase is determined by iteration and is indicated by the thick gray line in (c). As noted in the text, the isotope data and model results shown in (c) are detrended relative to the long-term linear trend in order to highlight small differences between the data and model results.

$$a_1 = \frac{A_{1f}}{A_{1s}} = \frac{(\lambda_{Sr}/2\pi L_{Sr})^2}{1 + (\lambda_{Sr}/2\pi L_{Sr})^2} \tag{9}$$

In this equation, A_f and A_s are the amplitudes of the sine curves for the fluid and solid, respectively. Rearranging Eq. (9) to solve for the reaction length produces the expression:

$$L_{Sr} = \frac{\lambda_{Sr}}{2\pi}\left(\frac{1-a_1}{a_1}\right)^{1/2} \tag{10}$$

Substituting $a_1 = 0.33$ yields a value of $L_{Sr} \approx 200$ meters. Using $M = 2.5$ ($\phi = 0.5$), $K_{Sr} = 20$, and $D_{Sr} = 7500$ m^2/Myr, we obtain $R = 0.005$ Myr^{-1} for the deep part of the Site 807A section (200–800 mbsf), which is about eight times smaller than for the upper 200 meters. Due to the various approximations employed, the uncertainty in the derived value of R is about ±50%.

5.3. Time-dependent numerical model for recrystallization rates

In this section, the estimates of recrystallization rates are refined using a time-dependent numerical model. We solve Eq. (1) using a modified centered finite difference approach similar to the one used by Richter and DePaolo (1987). As a result, the time-dependent evolution of a component, i, in the fluid is described by:

$$\frac{C_{if_j}^{n+1} - C_{if_j}^{n-1}}{2\Delta t} = \frac{D_s}{(\Delta z)^2}\left[C_{if_{j+1}}^{n} + C_{if_{j-1}}^{n} - C_{if_j}^{n+1} - C_{if_j}^{n-1}\right] - v\frac{C_{if_{j+1}}^{n} - C_{if_{j-1}}^{n}}{2\Delta z} + R_j M_j\left[C_{is_j}^{n-1} - K C_{if_j}^{n-1}\right] \tag{11}$$

where we solve for $C_{if_j}^{n+1}$ and i refers to either ^{86}Sr or ^{87}Sr. The isotopic evolution of the pore fluid is then the ratio of $^{87}Sr/^{86}Sr$ at any grid point, j. Since z is positive in the "up-core" direction, the reference grid counter j increases in the positive-z direction; thus $j+1$ is "up-core" relative to j. In addition, $v > 0$ indicates upwards advection. The parameter Δt is the time step used in the model calculation (in millions of years, Myr) while Δz is the grid spacing (in meters) of the finite difference solution in the z reference frame. If we set a grid point every 25 meters, $\Delta z = 25$ and is constant over the entire model space. To avoid numerical instability, Δt must be sufficiently small compared to Δz and D_s. In the model presented, stability is achieved if the condition $\Delta t \cdot D_s/(\Delta z)^2 \leqslant 0.5$ is met (Lasaga, 1998).

The reaction rate, R, is the parameter that is solved for using the numerical model. Previous work on deep-sea carbonate sections (Richter and DePaolo, 1988; Richter and Liang, 1993; Richter, 1996) shows that R is generally a function of sediment age. Our rough calculations presented above also suggest that R decreases with increasing sediment age at Site 807A. The functional form chosen by Richter and Liang (1993) to represent the variation of reaction rate with age is:

$$R(\text{age, Ma}) = \alpha + \beta e^{-\text{age}/\gamma} \tag{12}$$

where α is the background recrystallization rate at depth, $\alpha + \beta$ is the initial recrystallization rate, and γ is the rate at which the recrystallization rate changes with age. We adopt this functional form in our numerical model.

5.4. Estimates of D_{Sr} and K_{Sr}

The diffusion coefficient for Sr in solution is a function of temperature according to the relation:

$D^{o}_{Sr} = 3.69 \times 10^{-6} + 0.169 \times 10^{-6} T$ (°C), where D is in units of $cm^2\ s^{-1}$ (Boudreau, 1997). The temperature at the top of 807A is about 2 °C while at 820 mbsf the temperature is about 12 °C. This temperature difference corresponds to a variation in D^{o}_{Sr} of 4.0×10^{-6} to 5.7×10^{-6} from $z = 0$ to $z = 820$ mbsf. Boudreau (1997) showed that the diffusion coefficient in solution, D^{o}_{Sr}, can be used to calculate a diffusion coefficient in the sediment by correcting for tortuosity, $\theta : D^{sedt}_{Sr} = D^{o}_{Sr}/\phi^2$. The tortuosity can be related to the porosity (ϕ) by the relation, $\theta^2 \approx 1 - \ln(\phi^2)$. Given the porosity range (~0.7–0.5) from $z = 0$ to $z = 820$ meters at Site 807A (Fig. 3), the tortuosity correction varies between ~1.7 and 2.4. This corresponds to a diffusion coefficient in the sediment, D^{sedt}_{Sr}, that has a range from $z = 0$ to $z = 820$ mbsf of 2.35×10^{-6} to $2.40 \times 10^{-6}\ cm^2\ s^{-1}$. In this case, the decrease in porosity change with depth offsets the increase in D^{o}_{Sr} caused by the downhole increase in temperature. In our model, then, we use a depth-independent value for D^{sedt}_{Sr} of $2.4 \times 10^{-6}\ cm^2\ s^{-1}$ or $7500\ m^2$/Myr. The assumption of constant D^{sedt}_{Sr} with depth has been made in previous studies as well (Richter and DePaolo, 1987, 1988; Richter, 1993, 1996; Richter and Liang, 1993).

We consider two approaches to determining K_{Sr}. First, we calculate a depth-independent K_{Sr} value directly from the measured Sr concentrations of carbonates and pore fluids, as done by Richter and DePaolo (1987, 1988). We disregard the uppermost portion of the sedimentary column, which is not in exchange equilibrium because the pore fluids are affected by diffusive communication with the ocean. This approach yields K_{Sr} values of 18.54 ± 1.33 if all of the sediment below 200 mbsf is averaged, and 20.55 ± 1.40 if only the sediment below 600 mbsf is used.

Second, we calculate a variable K_{Sr} that is a function of the pore fluid Ca concentration. This approach is based on the work of Katz et al. (1972) and was also used by Richter (1996) in his modeling of diagenesis in deep sea carbonates. Temperature and pressure effects are not significant. Previous work has shown that temperature has a small effect on the K_{Sr} value for calcite (Katz et al., 1972), though no work has been done at the temperatures applicable to Site 807 (2–12 °C). In addition, while there are no experimental data at pressures greater than 1 atmosphere, equilibrium thermodynamic calculations for the reaction $CaCO_3 + Sr^{2+} \leftrightarrow SrCO_3 + Ca^{2+}$ (Johnson et al., 1992) indicate no change in the equilibrium constant over the range of pressures applicable at Site 807A. The primary influence on K_{Sr} is pore fluid Ca concentration. The relationship described by Katz et al. (1972) can be written:

$$K^{calcite}_{Sr} = \frac{m^{calcite}_{Sr}}{m^{calcite}_{Ca}} \cdot \frac{m^{fluid}_{Ca}}{m^{fluid}_{Sr}} \tag{13}$$

where m is the molar concentration of Sr or Ca in calcite (c) or fluid (f) and $K^{calcite}_{Sr}$ is the distribution coefficient. The expression for K_{Sr} can be rewritten to evaluate the effect of varying the Ca concentration of the pore fluid:

$$K^{c,n}_{Sr} = K^{c,m}_{Sr} \cdot \frac{m^{f,n}_{Ca}}{m^{f,m}_{Ca}} \tag{14}$$

assuming that the Sr/Ca ratio of calcite and the equilibrium concentration of Sr in the pore fluids are less variant than the Ca concentration through the sedimentary column. The simplified expression indicates that the difference between the K_{Sr} values at two depths (n and m) is directly related to the difference in pore fluid Ca concentration between these depths. We use our Ca model (Section 7) to constrain Ca concentrations in the pore fluids over time and calculate a K_{Sr} value at each model depth, referencing the K_{Sr} at all depths to the lowermost depth grid point in the model. The K_{Sr} value of this lowermost point (20.5) is constrained by the measured K_{Sr} values between 600 and 800 mbsf (20.55 ± 1.40) at Site 807A. As an example, we calculate the K_{Sr} value at the top of the column (0 mbsf) from the value at 780 mbsf:

$$K^{c,0m}_{Sr} = K^{c,780m}_{Sr} \cdot \frac{m^{f,0m}_{Ca}}{m^{f,780m}_{Ca}} = 20.5 \cdot \frac{10.6}{21.2} \approx 10.3 \tag{15}$$

In this example, the reference depth is taken to be 780 mbsf. In our model, the reference depth is 1350 mbsf. The pore fluid Ca concentrations at depths greater than 800 mbsf are constrained by either (1) deeper pore fluid data from 807C (to 1100 mbsf) or (2) linear extrapolation (to 1350 mbsf).

In considering values for K_{Sr} in our model, we do not explicitly consider the effect of celestite ($SrSO_4$) on pore fluid chemistry. Inclusion of celestite in a similar model (Richter, 1996) shows that the reaction rates derived from the model are not affected significantly for modest amounts of celestite precipitation, although the degree to which we successfully model the Sr concentration profile may be affected. We can estimate the degree of celestite saturation ($\Omega = [Sr^{2+}] \cdot [SO_4{}^{2-}]/K^{*}_{sp}$, where K^{*}_{sp} is the stoichiometric solubility product) at 807 using expressions for K^{*}_{sp} as a function of pressure, temperature, and salinity (Rushdi et al., 2000). It should be noted that the expressions for K^{*}_{sp} are derived for use in seawater and not sedimentary pore fluids. As a result, there may be some indeterminate absolute error associated with the estimates. Celestite is undersaturated in the upper 100 meters of the sedimentary column, reaches slight oversaturation between 100 and 500 mbsf ($\Omega < 1.25$), and becomes undersaturated again below 500 mbsf. Given the reported errors in the calculated K^{*}_{sp} value (Rushdi et al., 2000), the depth region between 140 and 220 mbsf is the only region of definite celestite oversaturation. Celestite saturation at 807 is similar to that of DSDP Site 516, as suggested by the modeling of Richter (1996). For 516, the derived reaction rate expression (as a function of age) was exactly the same with and without celestite in the model (Richter and Liang, 1993; Richter, 1996). Thus, the exclusion of celestite from our model should not affect the reaction rate that we derive.

5.5. The time-dependent depositional model

Our numerical model accounts for diffusion and reaction during the deposition of a 1350 meter sedimentary column at 25 meter grid spacing over a ~75 million year period. The model does not account for fluid advection. Richter (1993) pointed out that advection due to compaction is relatively minor and, therefore, is not critical to the model results. This is evident from the advective reaction length (v/RMK), which for $R = 10^{-8}\,\mathrm{yr}^{-1}$ and $v = 10$ m/Myr has a value of 37 meters. This is much smaller than the thickness of the sedimentary column. We also ignore externally imposed vertical flow through the sedimentary column. While Richter (1993) determined that advection velocities of 20–200 m/Myr are reasonable in some carbonate sections, there is no evidence from either Sr isotopes or concentrations that there is significant fluid flow at Site 807A. Fine-grained carbonate sediments like those of Site 807A generally have extremely low permeability and high hydraulic impedance relative to the underlying oceanic crust. If the sediment column is thicker than 300–400 meters, flow through the column can be projected from calculations to be chemically undetectable (Spinelli et al., 2004).

In the numerical model, the pore fluid is allowed to diffuse and react, subject to the boundary conditions described by Richter and DePaolo (1987, 1988). At $z = 0$, the concentration of ^{86}Sr is held constant (~91.3 μM) and the concentration of ^{87}Sr, $C_{87\mathrm{f}} = (^{87}\mathrm{Sr}/^{86}\mathrm{Sr})_t \cdot C_{86\mathrm{f}}$, where $(^{87}\mathrm{Sr}/^{86}\mathrm{Sr})_t$ is the Sr isotopic composition of seawater at some time, t, sampled from the global Sr seawater curve (DePaolo and Ingram, 1985; DePaolo, 1986; Hess et al., 1986; Richter and DePaolo, 1988; Capo and DePaolo, 1990; DePaolo and Finger, 1991). The Sr isotopic composition of the model sediment below 800 mbsf, which we did not measure, is estimated from the global seawater Sr isotope curve using the age model for 807C (Kroenke et al., 1991b). The Sr concentrations in the solid below 800 mbsf are assumed to be constant and equal to the average measured value in the section above 800 mbsf.

The Site 807 sedimentary section includes a low porosity layer below 1000 mbsf composed of chalk and chert (Gieskes and Lawrence, 1981). According to Gieskes and Lawrence (1981), this layer does not block diffusive communication between pore fluids below and above the layer, but it probably is another factor limiting fluid advection. In the numerical model, we do not explicitly account for this layer, but it should not significantly affect the results because we are mainly treating the sediment above 800 mbsf.

Best fits of the model to the data were determined by minimizing $\chi^2 = g(R) = g(f(\alpha,\beta,\gamma))$ in the upper 800 meters of the model column. A simplified χ^2 is written assuming zero (or small) x errors and Gaussian distribution of y errors:

$$\chi^2 = \sum_i \frac{(f(x_i) - y_i)^2}{\sigma_{y_i}^2} \tag{16}$$

where $f(x_i)$ is the y coordinate of the fit, y_i is the corresponding data point, and $\sigma_{y_i}^2$ is the error in each measurement of y_i. The maximum σ-error in the Sr concentration measurements is 2% (Delaney and Linn, 1993); thus the σ value assigned for the minimization of χ^2 is equal to the maximum error, or $0.02 \cdot y_i$. In order to match the model data to measured data prior to minimization, the measured data are linearly interpolated to the 25-meter grid spacing of the model. As part of the minimization routine, each parameter is varied and the minimum χ^2 found. In order to be confident in our solution, the minimization is run twice with different initial conditions. The first minimization utilizes initial values for α, β, and γ that are close to the likely values (based on previous modeling efforts such as Richter and Liang (1993)). The second minimization uses initial values near zero. This approach allows us to test whether or not the solutions converge given different initial conditions.

5.6. Validating the model—Site 590B with constant K_{Sr}

The depositional model was evaluated by applying it to data from DSDP Site 590B and comparing the results with those of Richter and Liang (1993). DePaolo (1986) originally reported the 590B ^{87}Sr/^{86}Sr pore fluid and carbonate data while Baker (1986) reported the pore fluid Sr concentration data from Site 590. Richter and DePaolo (1987) detailed the numerical modeling of the 590B Sr isotopic and concentration data, using a dynamic time-dependent diffusion-advection-reaction model. The main differences between the Richter and DePaolo (1987) model and our model is that the former model included compaction (and advection induced by compaction) at 1-meter grid spacing while ours ignores compaction and operates at 25-meter grid spacing.

Richter and DePaolo (1987) initially fit the pore fluid Sr data at Site 590B using a depth-dependent reaction rate term of the form $R(z, \mathrm{mbsf}) = 0.011 + 0.14\mathrm{e}^{-z/50}$. Richter and Liang (1993) subsequently used an age-dependent reaction rate at 590B, yielding the rate expression $R(\mathrm{age}, \mathrm{Ma}) = 0.0055 + 0.135\mathrm{e}^{-\mathrm{age}/2.1}$, where R has the units of Myr^{-1}. Using the same porosity-depth relationship ($\phi = 0.525 + 0.125\mathrm{e}^{-z/175}$), diffusion coefficient (2×10^{-6} $\mathrm{cm}^{-2}\,\mathrm{s}^{-1}$), Sr distribution coefficient (20), and rate-age expression as Richter and Liang (1993), we applied our depositional model to Site 590B.

The results of our model at 590B are shown in Fig. 4. The model Sr concentration profile captures the general trend of the Sr data but, as with the model of Richter and Liang (1993), it does not reproduce the maximum in Sr concentration near 100 mbsf or the fine features that occur below 100 mbsf. Our model also reproduces the 590B pore fluid ^{87}Sr/^{86}Sr data, within analytical error. The ^{87}Sr/^{86}Sr of the solid, which is tracked in the model, is determined by iteratively solving for the initial ^{87}Sr/^{86}Sr of the solid.

We conclude that our model, which has coarser grid spacing than Richter and Liang (1993) and ignores

compaction, fits the data as well as the Richter and Liang (1993) model and is sufficient for obtaining estimates of carbonate recrystallization rates from pore fluid data. The coarser grid spacing is expected to be sufficient because (1) the pore fluid data are widely spaced and (2) the pore fluid isotopic profile is expected to be smooth at the scale of the reaction length for Sr isotopes (50–100 meters at Site 590B).

6. Application of the model to site 807

The depositional model was applied to the pore fluid Sr concentration and isotopic data from Site 807A (Figs. 3e and g); the results are shown in Figs. 5 and 6. The best-fit curves were obtained by a three-step procedure in which the forward model is run and the parameters are adjusted iteratively. In the first step the pore fluid Sr concentration data are fit by minimizing χ^2, resulting in a first approximation for R(age). In the next step, the pore fluid $^{87}Sr/^{86}Sr$ data are fit by fine-tuning α, β, and γ using a second χ^2 minimization. The final step minimizes a χ^2 that is calculated using both the Sr isotopic and concentration data, ascribing equal weights to the misfits of each. The α, β, and γ parameters for the reaction term that are derived by following this minimization scheme at 807A are 0, 0.035, and 11. The α value is constrained partly by the model fit to the deepest pore fluid Sr concentration at nearby Site 807C (~788 μM at 1092 mbsf: Kroenke et al., 1991b). The choice of zero for α fits both this 1092 meter point and the Sr isotope data within analytical error.

Figs. 5 and 6 illustrate the sensitivity of the model to the parameters α, β, and γ. Figs. 5a–c demonstrate that a relatively high value of R is needed to fit the shallow pore fluid Sr concentration data, but a low value is needed to fit the deep pore fluid isotopic data. Figs. 5d–f show the effects of changing the absolute value of R while maintaining the same age-dependence. Figs. 6a–c show the effect of increasing the background value of R above zero, and Figs. 6d–f show the effects of changing the rate of decrease of R with age. Above 200 mbsf, both the isotope and concentration data suggest that a reaction rate of 3–4 %/Myr is appropriate. The age dependence required by the model results using a constant R (Figs. 5a–c) is suitably described by an exponential decrease with age, which produces reaction rates in the lower parts of the section that are ~10 times slower than those in the upper 200 meters. The estimated reaction rates and the difference in reaction rate between the uppermost part of the section and deeper parts of the section inferred from the depositional model are in excellent agreement with the rough values obtained from the steady-state models (Section 5.2).

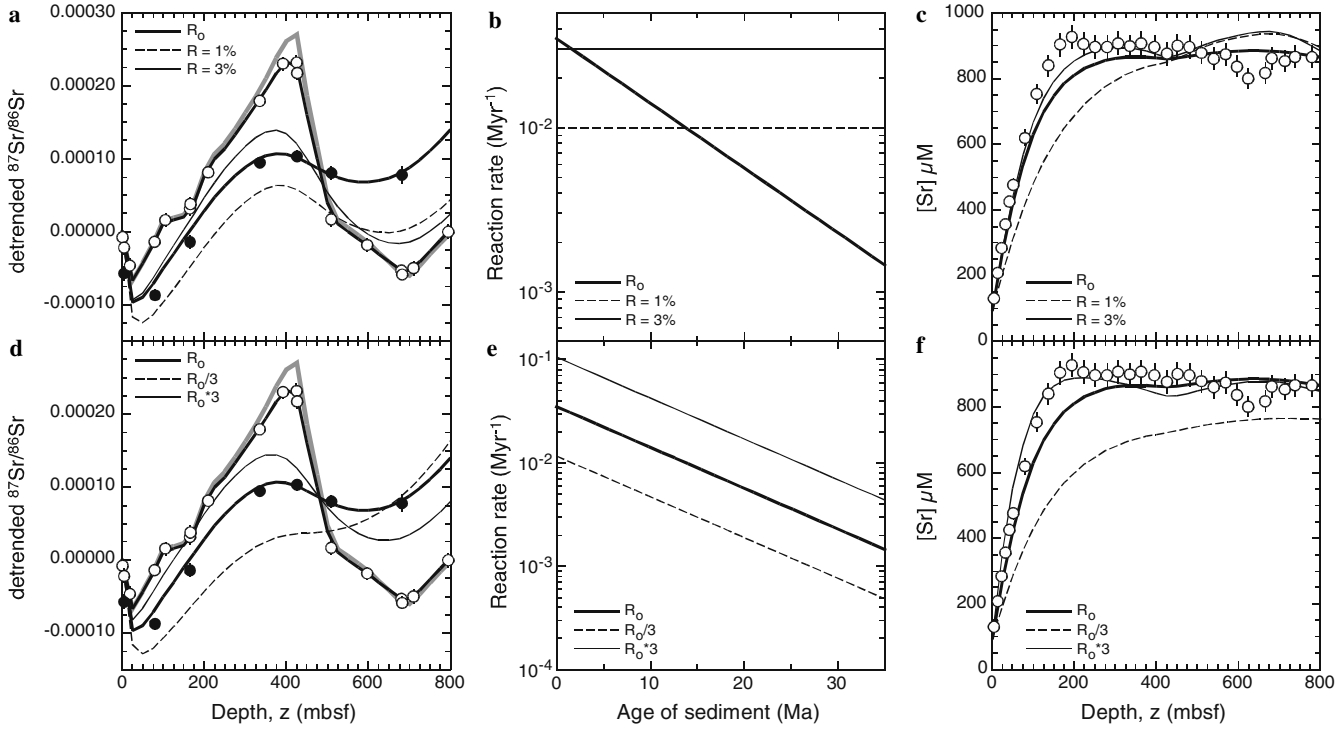

Fig. 5. Results of the depositional diffusion-reaction model at Site 807A. Results using a constant reaction rate as a function of depth are shown in panels (a–c). The model results for (a) $^{87}Sr/^{86}Sr$ in the column are visualized by detrending both the measured isotope data and model results relative to the long term linear trend in the carbonate $^{87}Sr/^{86}Sr$. The reaction rates used in the modeling are shown in (b), including the "best fit" R_o value for reference. The model results for (c) the pore fluid Sr concentration (μM) are also compared. Results using an age-dependent reaction rate (R_o) and varying it by a factor of 3 (equivalent to varying β by a factor of 3) are shown in panels (d–f). (d) The effects of varying R_o on the model $^{87}Sr/^{86}Sr$, (e) the resultant reaction rates, and (f) the effects of varying R_o on the model Sr concentration are illustrated. In all panels, the "best fit" R_o model is depicted with bold lines and the "best fit" parameters are denoted with "o" subscripts. In this constant K_{Sr} model, $K_{Sr} = 18$.

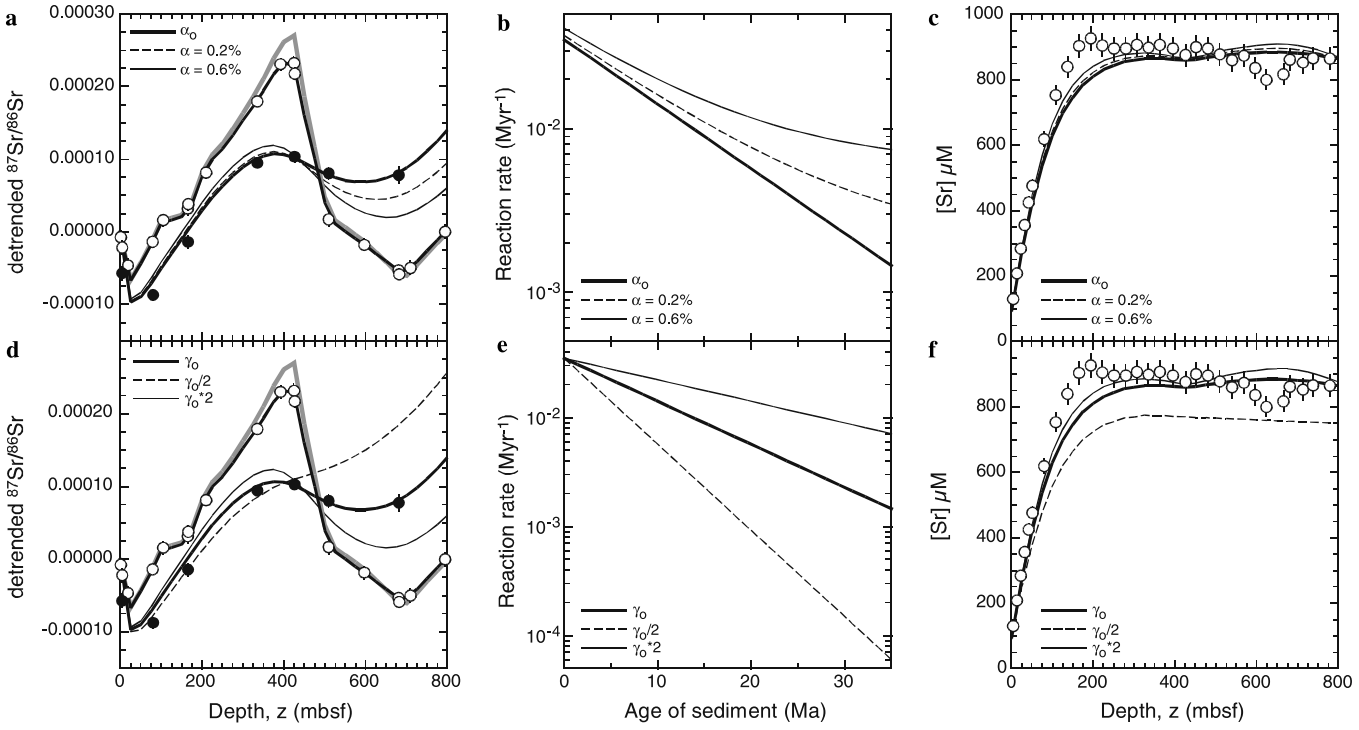

Fig. 6. Results of the depositional diffusion-reaction model at Site 807A. The effects of varying α are shown in panels (a–c). (a) The effects of varying α on the model $^{87}Sr/^{86}Sr$, (b) the resultant reaction rates, and (c) the effects of varying α on the model Sr concentration are illustrated. The effects of varying γ are shown in panels (d–f). (d) The effects of varying γ on the model $^{87}Sr/^{86}Sr$, (e) the resultant reaction rates, and (f) the effects of varying γ on the model Sr concentration (μM) are illustrated. In all panels, the "best fit" R_o model is depicted with bold lines and the "best fit" parameters are denoted with "o" subscripts. In this constant K_{Sr} model, $K_{Sr} = 18$.

The largest mismatch between model and measured pore fluid Sr concentration occurs at 100–200 mbsf, where the model does not capture the sharp maximum in the Sr concentration. The Richter and Liang (1993) model, which includes compaction and advection, resulted in a similar misfit of the Sr concentration profile at nearby DSDP Site 289 and at Site 590B. Therefore it is unlikely that the mismatch between our model and data at 200 meters is due to the absence of compaction-induced advection in the model. Instead, the mismatch could be due to (1) aragonite dissolution in young sediments, (2) a reaction rate that is not well characterized by an exponential function, or (3) a depth-variable distribution coefficient.

The presence of more reactive, Sr-rich aragonite in young sediments would increase the flux of Sr to the pore fluid from dissolution. Since aragonite can be more Sr-rich than calcite, including aragonite in young sediments is one way of increasing the Sr concentration in the pore fluid. However, there must be appreciable aragonite present down to 200 mbsf or so in order for this to be a viable explanation for the misfit between the Sr concentration data and the model fit in the upper 200 meters. X-ray diffraction analysis of the shallowest carbonate sample (0.95 mbsf) indicates that there is no measurable aragonite at this depth (<1 wt% detection limit). We conclude that it is unlikely that aragonite plays a significant role in the chemistry of Site 807A pore fluids.

6.1. Effect of variable K_{Sr} on the model results

The results of the variable-K_{Sr} model are shown in Fig. 7 for Sites 807A (a–c) and 590B (d–f). The inclusion of a variable K_{Sr} term in both cases results in a better fit to the Sr isotope (Figs. 7a and d) and Sr concentration data (Figs. 7c and f), especially in the upper 200 meters. At both 807A and 590B, slightly different rates of reaction are required for the "variable K_{Sr}" model, compared to the "constant K_{Sr}" model. For Site 807A, the "variable K_{Sr}" reaction rate expression is $0.023e^{-age/15.686}$, compared to $0.035e^{-age/11}$ for constant K_{Sr}. For Site 590B, a "variable K_{Sr}" rate expression of $0.0063 + 0.081e^{-age/2.13}$ is required, compared to the Richter (1993) expression of $0.0055 + 0.135e^{-age/2.1}$. The Site 590B model of Richter (1996) resulted in a rate expression of $0.0027 + 0.067e^{-age/2.1}$. The lower reaction rate calculated by Richter (1996) is mainly due to the use of a variable K_{Sr} value and an upward advection velocity of 75 m/Myr, and not the incorporation of celestite into the model.

The variable-K_{Sr} model results in generally lower reaction rates in the upper 100 meters of the sedimentary sections, and slightly smaller dependence of R on age. While the changes in the derived values of R are marginally significant, the variable-K_{Sr} model fits the data better than the constant-K_{Sr} model. We take the variable-K_{Sr} model to be the best representation of

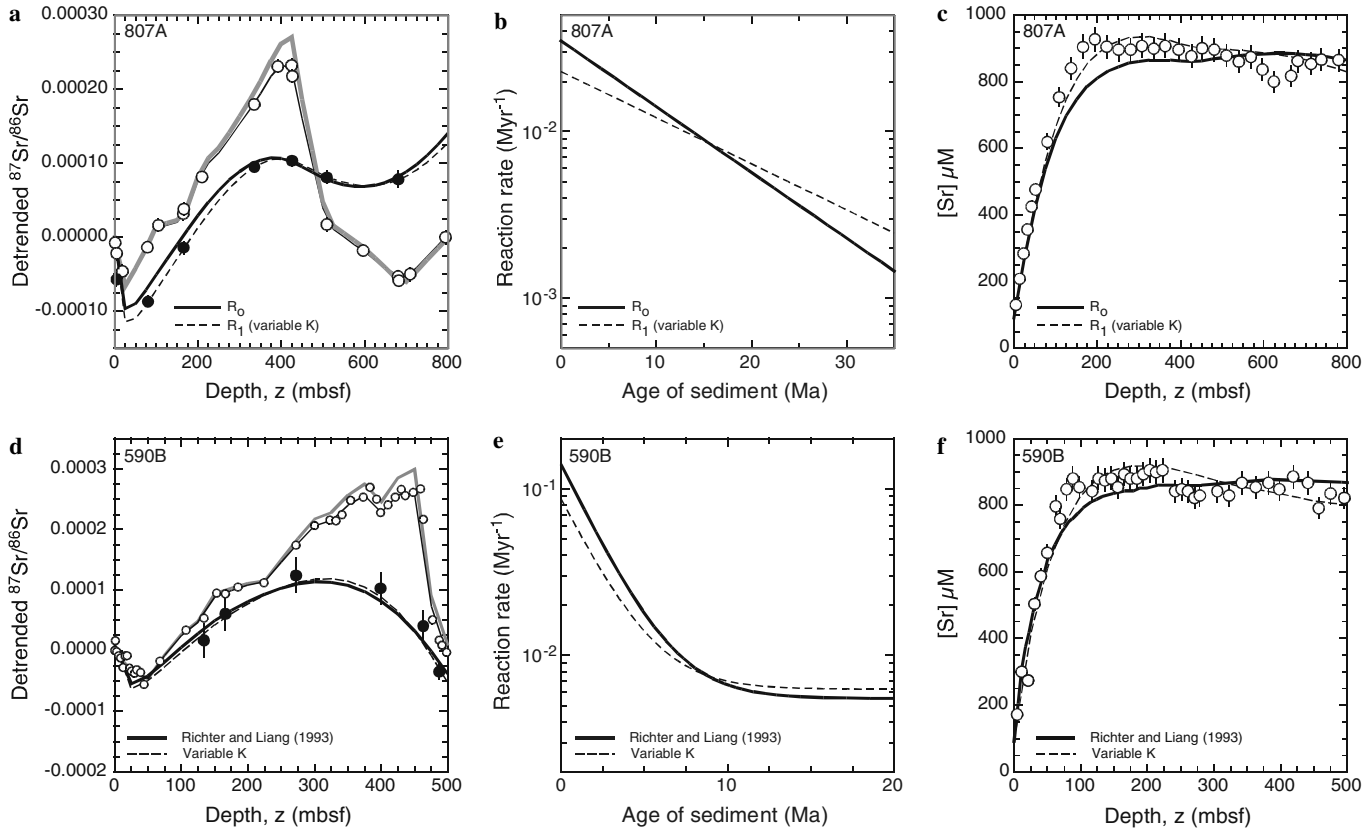

Fig. 7. Results of utilizing a K_{Sr} term constrained by the Ca concentration of pore fluids ("variable K_{Sr}" model) over the depositional history of the sedimentary column. Site 807A: (a) The Sr isotope data, (b) the derived reaction rate, and (c) the model fit to the Sr concentration (μM) profile are all affected by a variable K_{Sr} value. The model fit to the isotope and concentration data can be improved relative to the "constant K_{Sr}" model by using the age-dependent reaction rate term, $R_1 = 0.023e^{-age/15.686}$. Site 590B: (d) The Sr isotope data, (e) the derived reaction rate, and (f) the model fit to the Sr concentration (μM) profile are all affected by a variable K_{Sr} value. The reaction term which best fits the data is $R = 0.0063 + 0.081e^{-age/2.13}$. The model results from Richter and Liang (1993) are shown for comparison. The Ca concentrations of the pore fluids at each step in the model are constrained by a parallel Ca model that assumes local equilibrium in the sedimentary column. The equilibrium constants in the Ca model are calculated from the measured Ca pore fluid data as a function of depth.

the carbonate recrystallization rates at both Site 807 and Site 590B.

6.2. Comparison to previous estimates of reaction rates

The age-dependent reaction rate at Site 807A determined from our variable-K_{Sr} model can be compared to the relationships determined for other carbonate cores (Richter and Liang, 1993). Nine carbonate-dominated DSDP sites were previously investigated and modeled, using Sr concentrations and isotopes to constrain reaction rate as a function of age (Richter and Liang, 1993; Richter, 1996). Of these nine sites, only three (DSDP Sites 289, 516, and 593) extend back in time as far as 807A. Of these three, both 516 and 593 suggest low background recrystallization rates (<0.2%/Myr), in agreement with our results at 807A. Richter and Liang (1993) inferred slightly higher background recrystallization rates for Site 289, but the pore fluid isotopic data are not fit well by the model at any depth, and the deepest samples may be affected by the lower boundary condition. For Sites 575 and 590B, the recrystallization rates are not well constrained for sediment ages greater than about 15 Ma. Our results for Site 807A, in concert with those for Sites 516, 593, and 289, suggest that carbonate recrystallization rates continue to decrease as the sediment ages, at least up to ages of about 35 Ma. For Site 807, the deep pore fluid sample at 1092 meters suggests that the recrystallization rate continues to decrease to a sediment age of about 50 Ma.

As noted by Richter (1996), the reaction rate calculated for Site 590B is anomalously high, even after downward corrections for variable K_{Sr} and the presence of celestite. The other sites that have been studied yield initial rates of order 2–3%/Myr, whereas Site 590B has an initial rate closer to 10%/Myr. This difference is evident without detailed modeling from the pore fluid Sr concentration profiles. For Site 590B, the value for L_{Sr} (40 meters) is about one-half that for Site 807, which requires a reaction rate that is about 4 times higher. Correction for a depth-variable K_{Sr} and upward velocity of 75 m/Myr at 590B makes the inferred 590B rates about three times higher than those for Site 807A, which is precisely what the more detailed numerical modeling suggests.

7. Implications of site 807A carbonate recrystallization rates

7.1. Ca concentration profile of Site 807A pore fluid

The Sr concentration profile of the Site 807A pore fluids indicates that the diffusive reaction length for Sr (L_{Sr}) is about 80–100 meters in the upper 200 meters of the section and is about 200 meters in the deeper parts of the section. Using the reaction length for Sr, we can calculate the reaction length for Ca:

$$L_{Ca} = \left(\frac{D_{Ca}}{RMK_{Ca}}\right)^{1/2} \xrightarrow{\text{which leads to}} \frac{L_{Ca}}{L_{Sr}} = \left(\frac{D_{Ca}}{D_{Sr}}\frac{K_{Sr}}{K_{Ca}}\right)^{1/2} \quad (17)$$

An analysis similar to that done for D_{Sr} suggests that $D_{Ca} = D_{Sr} = 7500\ m^2/Myr$, so that the only difference between L_{Ca} and L_{Sr} is the difference between K_{Sr} and K_{Ca}. At the top of the column, the value for K_{Ca} is about 900. Thus, the reaction length for Ca is smaller than that for Sr by a factor of $(20/900)^{1/2}$, or 0.14. Hence, the reaction length for Ca is 11–14 meters for the top part of the column. This means that (1) the pore fluid Ca concentration must reach the equilibrium value at about 30 mbsf and (2) the pore fluid Ca concentrations below 30 mbsf must be equilibrium values. The reaction length for Ca increases to about 30–35 meters deeper in the column where the reaction rates are lower, but the reaction rates are still fast enough to maintain the pore fluid concentrations at the equilibrium values.

The pore fluid Ca concentration profile looks much different from the Sr profile because the local bottom waters and the carbonate sediments are not far out of equilibrium, with respect to Ca, at the sediment–water interface. In the Pacific Ocean, water at depth greater than 1000 meters is generally near or at saturation with respect to calcite (Millero, 1996). At Site 807A the seafloor is at ~2800 meters, which is close to the average depth of the calcite lysocline (3000–4000 meters) in the Pacific Ocean (Millero, 1996). So while Sr has an equilibrium pore fluid concentration that is 10 times higher than the seawater value, making the effects of calcite recrystallization on pore fluid Sr concentrations easy to detect, Ca has an equilibrium pore fluid concentration that is close to the initial pore fluid (i.e., bottom water) concentration. As a result, it is impossible to detect the effects of calcite recrystallization from the pore fluid Ca concentration gradient in the upper 5–30 meters of the section.

The pattern of generally increasing Ca concentration with depth is a common feature of pore fluids from most carbonate-dominated sections (McDuff and Gieskes, 1976; Gieskes and Lawrence, 1981; Baker et al., 1991). Towards the bottom of the sampled portions of these carbonate-dominated sections, two types of Ca profiles are observed: those that increase strongly and those that reach a near-zero slope at depth. Sites with the former type of profile (DSDP Sites 285, 315, and 317: Gieskes and Lawrence, 1981) are influenced by a diffusive flux of material from below, derived from weathering of silicates (basalt, volcanic glass, and/or clastic sediments) at depth. Sites with the latter profile, such as ODP Site 807 and DSDP Sites 516 and 590 (Baker, 1986), are usually interpreted as having little silicate influence from below. In the Site 807 section it is clear that there is no significant Ca source at depth, since the derivative of the Ca concentration with depth is close to zero at about 1100 mbsf.

7.2. Calculated pH and CO_3^{2-} profiles

Our results for the carbonate recrystallization rates at Site 807A *require* that the pore fluid Ca profile is controlled by calcite solubility, not by sources and sinks of Ca in or below the sediment column. The requirement of equilibrium between calcite and pore fluid below 30 mbsf allows us to calculate the corresponding equilibrium concentration of CO_3^{2-} in the pore fluids, using pressure- and temperature-corrected equilibrium constants. Then using the calculated CO_3^{2-} concentration and measurements of total alkalinity, we calculate the *in situ* pore fluid pH according to:

$$[H^+] = \frac{A_c K_2^* - [CO_3^{2-}]_{eq} 2K_2^*}{[CO_3^{2-}]_{eq}} \quad (18)$$

where K_2^* is the equilibrium constant for the reaction, $HCO_3^- \leftrightarrow CO_3^{2-} + H^+$. The carbonate alkalinity, A_c, is related to the total alkalinity, TA, that is directly measured in the pore fluids. After correcting the necessary equilibrium constants for temperature and pressure, A_c is calculated by $TA - \sum B_i$, where $\sum B_i$ are the bases other than bicarbonate and carbonate ion that contribute to total alkalinity. We adjust TA for $B(OH)_4^-$ and $SiO(OH)_3^-$, correcting for temperature and pressure in the former case and temperature in the latter one (Millero, 1995). We ignore the effect of minor bases such as HS^- and HPO_4^{2-}. Overall, the $\sum B_i$ correction is small and affects the calculated pH by less than 0.01 log units. In addition, we point out that the measured alkalinity is rather high at ~4.5 mbsf (3.5 mM) compared to that of seawater (~2.5 mM). Pore fluid alkalinities in the upper 6 meters of similar carbonate-rich sedimentary columns are in the range 2.7–3.1 mM (Bralower et al., 2002) so the alkalinity at 807A is not anomalous. If the carbonate recrystallization rates in the uppermost few meters of the sediment are even higher than our estimates for the top 20 meters, then the pore fluids can be different from seawater even at a depth of 4.5 mbsf.

It should be noted that the equilibrium constants used in our calculations are appropriate for use in solutions with chemical compositions similar to that of seawater, over pressure-temperature-salinity conditions encountered in the ocean. We apply them to the sedimentary section with the knowledge that this is the case and that, as a result, our calculations contain some amount of indeterminate absolute error. Also, the scale on which the measured pH values are reported should be the "free" pH scale (Gieskes et al., 1991) while the calculated pH values refer to the

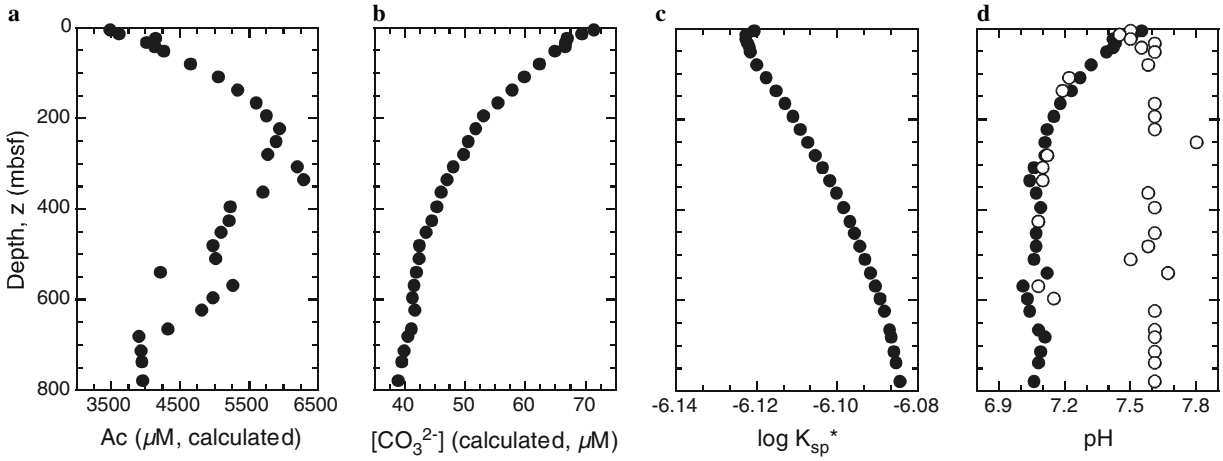

Fig. 8. (a) The carbonate alkalinity, A_c (μM), calculated from Site 807A total alkalinity (TA) measurements using temperature- and pressure-corrected equilibrium constants (Millero, 1982; Millero, 1995; Millero, 1996). (b) The concentration of carbonate ion (μM) in equilibrium with the measured Ca^{2+} (controlled by calcite solubility: $K^*_{sp}/[Ca^{2+}]_f$. (c) The temperature- and pressure-corrected solubility product (K_{sp}) and (d) the pH (●) calculated using the (a) A_c and the (b) equilibrium CO_3^{2-} concentration. The calculated pH (●) is compared to the measured pH (○) at Site 807A to illustrate the agreement between the measured and the calculated pH in about 30% of the measurements. The scales of the two measurements may be different by as much as 0.05 log units, accounting for some of the observed mismatch.

"total" pH scale. The "free" and "total" scales are related by: $pH_{TOTAL} = pH_{FREE} - \log(1 + \beta_{HSO_4^-}[SO_4^{2-}])$, where β is the association constant for HSO_4^- and is calculable (Dickson, 1990) and $[SO_4^{2-}]$ is the concentration (moles/kg solution) of sulfate ion in solution (Millero, 2001). For temperatures between 2 and 12 °C, sulfate concentrations between 21 and 28 mM, and ionic strengths between 0.7 and 1, the two pH scales differ by less than 0.05 log units.

For Site 807A, we calculate a steady decrease in CO_3^{2-} concentration (Fig. 8b) and in pH (Fig. 8d) in the upper 300 meters of the sedimentary column. The decrease in pore fluid pH coincides with an increase in carbonate alkalinity and a decrease in both CO_3^{2-} and SO_4^{2-} concentrations. The alkalinity increases until about 300 mbsf, the same depth at which the SO_4^{2-} decrease halts. This suggests some link between the two, such as microbial sulfate reduction (Mitterer et al., 2001; Morse, 2002). There is not an abundant amount of organic carbon present (<0.4% in the upper 200 meters), though Mitterer et al. (2001) previously showed that microbial sulfate reduction occurs in carbonate-dominated sediments containing less than 1% organic carbon. As at 807A, the pore fluid sulfate profile in Mitterer et al.'s (2001) study generally decreased from a relative high in the upper 50 meters to a minimum near 300 mbsf.

The pH decrease with depth that we calculate is typically attributed to calcite precipitation according to the reaction (e.g., Maher et al., 2006):

$$Ca^{2+} + HCO_3^- \leftrightarrow CaCO_3 + H^+ \quad (19)$$

Even though there is a 50% *increase* in pore fluid Ca^{2+} concentration with depth, we conclude that there is in fact a small amount of *net calcite precipitation* (and not dissolution) from the pore fluids that accounts for the observed decrease in pH with depth.

The measured pH profile at Site 807A matches our calculated pH curve for 11 of the 31 samples measured on-board (Fig. 8d). The measured distribution of pH has a peculiar pattern that must be a result of artifacts. The distribution of pH values is bimodal, with most of the values distributed near 7.6, and, as a result of the bimodal distribution, there are sharp pH gradients. Considering the relatively smooth variations in both alkalinity and Ca^{2+} concentration in the pore fluid, there is no reason to expect an oscillatory pH pattern. Also, the sharp pH gradients could not be maintained against diffusion. Apparently, the pH measurements that yielded a value of 7.6 are incorrect and probably reflect reequilibration of the pore fluids with atmospheric CO_2 prior to measurement. The degree of reequilibration does not appear to be related to reaction occurring during the raising of the core sample from depth to the surface, since there is no correlation with depth. Perhaps those pore fluids where the pH measurement was performed soon after squeeze-cake sampling are close to correct, while those samples measured after longer reequilibration times are incorrect. If we reequilibrate a model solution with similar chemistry as the Site 807 pore fluids with atmospheric CO_2 ($pCO_2 = 3.87 \times 10^{-4}$ bar) in equilibrium with calcite, we obtain a pH of about 7.7 (Steefel, 2001). This is similar to the measured pH (~7.6) in the samples that we argue are affected by reequilibration. Similar problems with on-board pH measurements have been noted in other ODP pore fluids. Maher et al. (2006), for example, conclude that *none* of the measured pH values at Site 984 are representative of *in situ* conditions in the pore fluid.

7.3. Mg concentration profile for Site 807A pore fluid

Evaluation of the pore fluid Mg concentration profile at 807A (Fig. 3d) requires values for D_{Mg} and K_{Mg}. Our

analysis of the available data suggests that the diffusion coefficient for Mg can be considered constant and equal to ~6900 m^2/Myr (Boudreau, 1997). The distribution coefficient for Mg (K_{Mg}) between calcite and solution has been investigated experimentally (Katz, 1973; Mucci and Morse, 1983; Oomori et al., 1987; Huang and Fairchild, 2001) and is found to vary between ~0.1 and 0.6 at $T < 25$ °C and one atmosphere pressure. Using a nominal value of $K_{Mg} = 0.4 \pm 0.2$, we find that the reaction length for Mg is in the range $L_{Mg} = 1100$–2000 meters. This result indicates that the pore fluid Mg concentration is weakly affected by calcite recrystallization and, therefore, we do not expect the pore fluid Mg concentration to be in equilibrium with calcite at any depth in the sedimentary column.

The large value of L_{Mg} implies that the decreasing pore fluid Mg concentrations at 807A are due either to a Mg-sink within the sediment column or to variations in the upper and/or lower boundary conditions. One possible sink for Mg is the precipitation of secondary clay minerals derived from the weathering of primary silicate minerals. However, Site 807 sediments contain only traces of primary silicate minerals (Krissek and Janecek, 1993), and the rate constants for both silicate mineral dissolution and clay formation are typically several orders of magnitude smaller than those for calcite recrystallization (Maher et al., 2006). We therefore conclude that Mg-clay precipitation has a negligible effect on the pore fluid Mg concentrations. Additionally, it appears that the lower boundary of the sediment column has not changed, since the pore fluid Mg concentration gradient in the deepest part of the section sampled at Site 807 is close to zero.

Accordingly, the most likely explanation for the Mg depth profile is that the upper boundary condition has changed. In particular, the data require that the seawater Mg concentration has increased over the past 40 million years. Zimmermann (2000) and Horita et al. (2002) report data on fluid inclusions in evaporite deposits that suggest that seawater Mg has increased significantly (10–15 mM) over the past 20–40 million years. Berner (2004) also suggests that seawater Mg has increased over the past 40 million years, based on modeling of the global Mg, Ca, and sulfate cycles. The idea that pore fluids may retain some memory of seawater Mg concentration over time is supported by considering the diffusive adjustment time, calculated to be $L^2/D_{Mg} \approx 100$ million years, for pore fluid Mg in the 800 meter section at 807A. This analysis suggests that the pore fluid retains memory of changes in the seawater Mg concentration over at least the past 10–20 million years. In the next section we use our depositional model to evaluate how well the Site 807A pore fluid Mg data constrain paleo-seawater Mg concentration.

7.4. Model for Neogene seawater Mg concentration changes

For the Mg numerical model, we formulate K_{Mg} in a similar manner as K_{Sr} (Section 5.4):

$$K^{c,n}_{Mg} = K^{c,m}_{Mg} \cdot \frac{m^{f,n}_{Ca}}{m^{f,m}_{Ca}} \tag{20}$$

Using this formulation, we must select a reference value for K_{Mg} at depth. Unfortunately, there are no experimental data at pressures higher than one atmosphere upon which to base this value, and we cannot use the deep pore fluid Mg concentrations because they cannot be expected to be in equilibrium with calcite. Oomori et al. (1987) and Huang and Fairchild (2001) found that K_{Mg} decreases with decreasing temperature (in the range 10–50 °C), so that we would expect K_{Mg} to be smaller in the section at 807A (~2–12 °C) than at 25 °C. The effect of pressure on K_{Mg} is poorly constrained. Thermodynamic calculations of the equilibrium constant for the reaction (Johnson et al., 1992):

$$Mg^{2+} + CaCO_3 \leftrightarrow Ca^{2+} + MgCO_3 \tag{21}$$

at pressures relevant to 807A suggest that the equilibrium constant increases by ~40% down section (increasing temperature and pressure), indicating that K_{Mg} increases slightly with pressure. Based on this analysis, we investigate three K_{Mg} values (0.4, 0.6, and 0.84) in order to illustrate how the uncertainty in K_{Mg} affects our determination of seawater Mg over time. The first two values investigated represent estimates for K_{Mg} in the sedimentary column while the third value is calculated from measured Mg concentrations in pore fluids and calcite below about 800 meters depth (0.84 ± 0.04). The third value is therefore as close to an empirically-derived value for K_{Mg} as we can get. The average calcite Mg content of deep samples (>800 mbsf) is 0.032 ± 0.002 molal while the Mg content of the entire section at 807A ranges between 0.022 and 0.048 molal. The Mg contents of calcite at 807 show no significant or systematic changes with depth that would support the use of a model in which the solid Mg content varied (Delaney and Linn, 1993).

For each of the reference K_{Mg} values, we calculate K_{Mg} as a function of pore fluid Ca concentration in each time step of the model (Fig. 9a). Our initial guess for the seawater Mg curve assumes that the present relationship between pore fluid Mg concentration and sediment age is the same as the relationship between seawater Mg concentration and age. We then adjust our initial guess for the seawater Mg concentration curve iteratively until we find the initial Mg concentration versus age relationship that results in a final Mg concentration profile identical to the measured profile. By doing this with each of the three values of K_{Mg}, we retrieve a range of initial Mg concentration profiles (Fig. 9b) that fit the measured pore fluid Mg concentrations to the same degree (Fig. 9c). Fig. 9b shows that varying K_{Mg} by 0.2 changes the inferred seawater Mg concentration at the time of deposition of the sediment at 800 m depth by <10%. Another aspect of the sensitivity of the model is shown in Fig. 10. For a given value of K_{Mg}, the inferred initial pore fluid Mg concentrations are fixed within about 2% by the data.

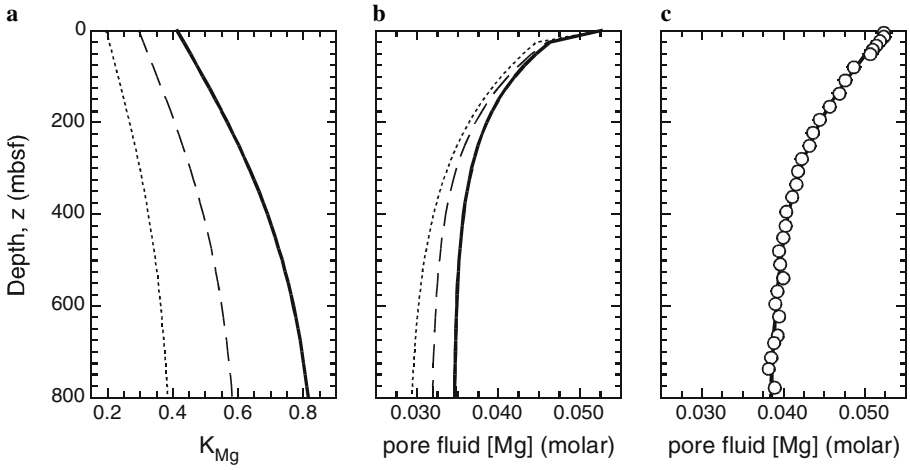

Fig. 9. Results of applying the depositional model to the pore fluid Mg profiles at Site 807A. The K_{Mg} values used to model Mg in the sedimentary column are shown in (a). A range of values is used to demonstrate how uncertainty in this parameter affects the determination of the initial Mg profile, (b) The initial Mg profiles solved for using our model, applying the various K_{Mg} values shown in (a). Given the range of K_{Mg} values used, the final Mg profiles (c) fit the measured Mg pore fluid data to the same degree.

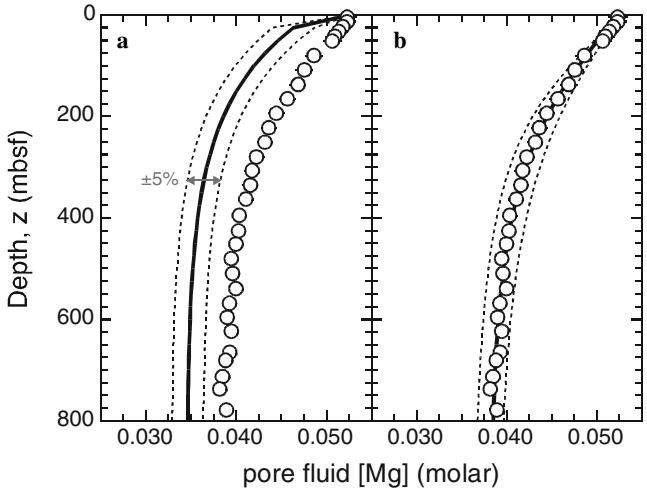

Fig. 10. The sensitivity of the Mg model to the initial condition, (a) Varying the initial Mg profile (——) by ±5% (– – –) results in (b) unacceptable fits to the measured pore fluid Mg data (○). As a result, the initial Mg profile that is solved for in the model is relatively precise (<2%), given the analytical uncertainty of the measured pore fluid Mg concentrations at 807A (Kroenke et al., 1991a).

It is important to keep in mind that the pore fluids retain only the long-term trend of the Mg concentration in the initial pore fluid. Fluctuations in seawater Mg concentration on short timescales are lost as a result of diffusive effects in the pore fluid. The smoothing effect of diffusion on the signal is proportional to the inverse square of the wavelength. Therefore, the timescale for smoothing variations with a wavelength of 100 meters is about 1.5 million years, while the timescale for smoothing variations with a wavelength of 200 meters is about 6 million years. However, because Mg has a very long residence time in seawater—about 22 million years—short timescale fluctuations are not expected to have significant amplitudes anyway.

Another consequence of the long residence time of Mg in seawater is that the Mg concentration of seawater is uniform globally. Thus, a temporal record of seawater Mg concentration derived at a single location sufficiently describes the entire ocean. As a result, the age-depth relationship at 807A for the initial pore fluid (Fig. 9a) can be translated into a *global* seawater Mg versus age curve for the past 40 million years (Fig. 11). The model results are evaluated against the available data from fluid inclusions in halite (Zimmermann, 2000; Horita et al., 2002). Fig. 11a shows that while the measured Site 807 pore fluid Mg data are in reasonable agreement with the evaporite data, the model-derived initial pore fluid Mg concentrations are generally on the low side of the evaporite data. Fig. 11b shows the result if a "best fit" to the evaporite data is used to set the initial pore fluid compositions in the model. This approach results in a model pore fluid Mg profile that does not agree with the pore fluid Mg measurements. The evaporite-based model could be made to work if the K_{Mg} value were increased to a value larger than 0.84. However, there is no evidence either from experiments or from the measured Mg contents of calcite at 807A (Delaney and Linn, 1993) that K_{Mg} is larger than 0.84 under the temperature–pressure conditions observed at 807A. The initial Mg content of the solid phase used in the model also has a significant effect on the final result (Fig. 11c). In Figs. 11a and b, we use the average measured value for Mg in carbonate from the Site 807A core as the initial Mg concentration in freshly deposited calcite (0.034 mol Mg/kg calcite). If we vary the calcite Mg content of the initial carbonate over the range observed for calcite at Site 807A, a range of seawater Mg concentration curves results. The result is that varying the initial Mg content of calcite from 0.022 to 0.048 molal has a similar effect as varying K_{Mg} between 0.4 and 0.84. The observation remains, however, that within the range of calcite Mg

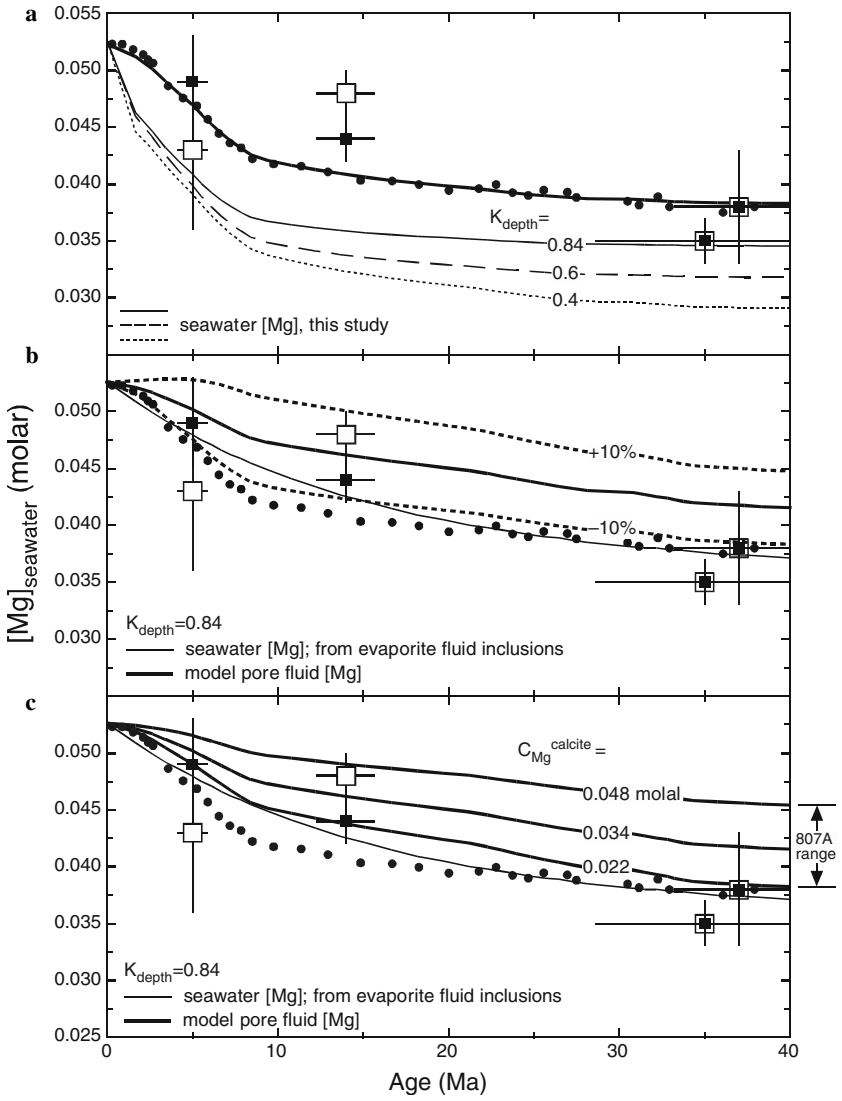

Fig. 11. Seawater Mg curves for the past 35 million years, as determined by Mg modeling, compared to seawater Mg data from fluid inclusions in evaporites. The evaporite fluid inclusion data are designated by ■ (Zimmermann, 2000) and □ (Horita et al., 2002) in all panels. All initial Mg curves are displayed with thin, solid or dashed lines while all final model curves are displayed with bold solid or dashed lines, (a) Our seawater Mg curve is constrained by the measured pore fluid and calcite Mg concentrations and the numerical model. K_{Mg} is varied over a reasonable range in order to illustrate the effect of uncertainty in this parameter upon our seawater Mg curve, (b) A seawater Mg curve defined by the evaporite data (—) does not fit the measured pore fluid data at 807A, even considering the large uncertainty (~10%) in the evaporite-based Mg data, (c) The effect of the calcite Mg concentration on the fit to the measured pore fluid data, using the evaporite-based seawater curve as an initial condition.

contents at 807, the evaporite data do not produce a pore fluid Mg curve that agrees with the measured data at 807A.

The seawater Mg concentration curve we retrieve from the Site 807A pore fluid data (Fig. 11a; $K_{Mg} = 0.84$) matches well with the data from evaporite inclusions for the youngest and oldest evaporite samples in the age range of our model (5 and ~35 Ma) but does not fit the data for the ~14 Ma evaporites. Taken at face value, our curve suggests that seawater Mg increased minimally between 35 and 10 Ma and then increased quite rapidly since 10 Ma from about 35 mM to the modern value of 52 mM.

The features of our derived seawater Mg curve can be understood by considering the controls governing the Mg concentration of seawater (Berner, 2004). Weathering and dissolution of old dolomite and Mg-silicates provides Mg to the ocean while hydrothermal alteration and weathering of seafloor basalt remove Mg, in exchange for Ca, from the ocean. Magnesium is also removed by coprecipitation with calcite, but this is a small flux relative to the primary fluxes mentioned above. A rise in seawater Mg concentration suggests an increase in the weathering flux, a decrease in the removal rate, or both. If the removal rate is tied to seafloor spreading processes, the relatively long timescale for tectonic changes makes it unlikely that a rapid rise in Mg could occur over the past 10 million years as a result of a change in the removal rate. Therefore, the most likely explanation for the change in seawater Mg concentration is an increase in the weathering flux of Mg. An enhanced

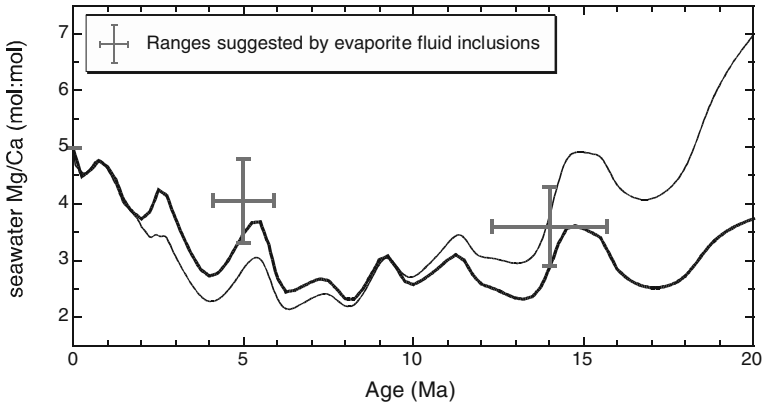

Fig. 12. The Mg/Ca ratio in seawater over the past 20 million years, as suggested by evaporite fluid inclusions (Lowenstein et al., 2001; Horita et al., 2002) and the combination of results from this study and Fantle and DePaolo (2005). The two curves shown are calculated from the seawater Mg curve in this study (Fig. 11a; $K_{Mg} = 0.84$) and the marine Ca curves in Fantle and DePaolo (2005), for the two cases ($\delta_W = -0.48$ and variable δ_W) shown in Fig. 3b of that study.

weathering flux could be caused by (1) a general increase in erosion rates or (2) an increase in the weathering of dolomite specifically over the past 10 million years. Evidence suggests that global erosion has indeed increased over the past 5 million years (Hayes et al., 1988; Molnar, 2004). In addition, increased continental ice cover and lower sea level over the same time interval could expose more dolomite on low-lying continental areas to erosion.

If we combine the seawater Mg curve derived in the current study with the 20 million year seawater Ca curve of Fantle and DePaolo (2005), we can construct a seawater Mg/Ca curve for the past 20 million years (Fig. 12). The resultant Mg/Ca curve, which agrees with the seawater Mg/Ca suggested by measurements of evaporite fluid inclusions (Lowenstein et al., 2001; Horita et al., 2002), suggests decreasing or relatively constant seawater Mg/Ca from 20 to 13–14 Ma, generally constant Mg/Ca between 13 and 7 Ma, and rising seawater Mg/Ca over the past 7 million years. The significant peaks in Mg/Ca at 5–6 and ~15 Ma, which correspond to the end of an episode of enhanced Tibetan Plateau uplift and the beginning of ice sheet growth in East and West Antarctica, respectively (Zachos et al., 2001; Fantle and DePaolo, 2005), can be viewed as support for our assertion that changes in weathering, driven by continental tectonics and climate, play a dominant role in the evolving Mg–Ca chemistry of the global ocean.

7.5. Reaction rate as a function of age

The pore fluid Sr concentration and isotopic data from Site 807A confirm the conclusions from previous work that the recrystallization rate of carbonate sediments decreases with age (Richter and Liang, 1993). In contrast to previous work, we show by detailed examination of the pore fluid isotopic data that the recrystallization rate continues to decrease throughout the 30-plus million year sedimentary record at Site 807, rather than decreasing rapidly in the first few million years and reaching a constant background value (Richter and Liang, 1993).

The age-dependence of mineral-fluid reaction rates has also been discussed in the literature with respect to irreversible weathering of silicate minerals in soils and deep-sea sediments (Taylor and Blum, 1995; White et al., 1996, 2001; White and Brantley, 2003; Maher et al., 2004, 2006). The rate-age relationship suggested by Maher et al. (2006) is shown in Fig. 13 along with calcite recrystallization rates determined in this study and in other deep-sea carbonate sediments. Data from soils is restricted to ages of less than 1 Ma while the data from deep-sea carbonates is limited to ages greater than a few million years. The lower age limit for carbonates is imposed by the reaction length for Sr. The Sr pore fluid data tend to average the recrystallization rate over a lengthscale equal to L_{Sr}, which is 40–100 meters in the sites studied. The sedimentation rate is typically 20 m/Myr, so the "initial" recrystallization rate we calculate (equal to $\alpha + \beta$ in our parameterization of reaction rate) applies to sediments that have an average age of 2–5 Ma. The recrystallization rate may be higher in the youngest sediment in the uppermost 10 meters of the section, but the effects of these higher rates cannot be discerned in the Sr data.

Maher et al. (2004, 2006) investigated "young" sediments at Site 984 using U isotopes and reactive transport modeling, and estimated the calcite recrystallization rate in 0.1–0.4 Ma sediments to be 60%/Myr (Fig. 13). This rate is about 15–20 times higher than the maximum inferred from Sr isotopes in the present study, but the sediments examined at Site 984 are also 15–20 times younger than the 807A sediments we investigate using Sr isotopes. If we assume that the Maher et al. (2006) rates apply to young sediments at Site 807A (uppermost 10 meters), then the reaction length for Ca in the upper few meters of sediment would be only 3–4 meters. This, in turn, means that pore fluid Ca must be in equilibrium with calcite everywhere in the sedimentary section below 8–10 mbsf.

An intriguing, but difficult to understand, aspect of the data in Fig. 13 is that the carbonate recrystallization rates are on the same trend as the weathering rates of silicate

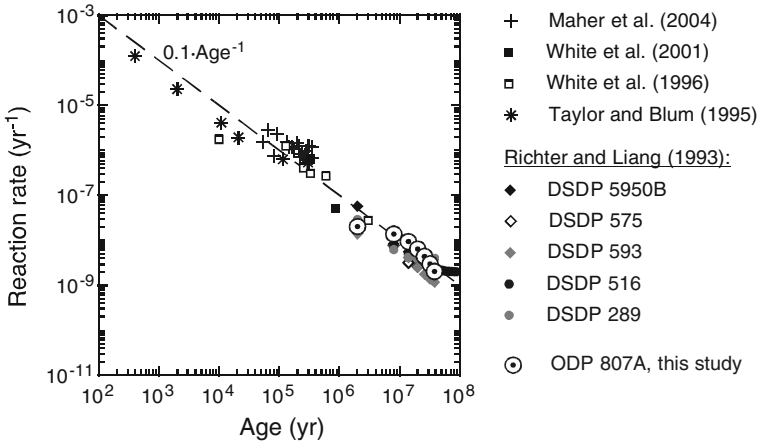

Fig. 13. Reaction rate (yr^{-1}) as a function of age (yr). The reaction rate data for 807A are plotted along with the $Rate = 0.1 \cdot Age^{-1}$ relationship suggested by Maher et al. (2004). The rates for 807A sediments are derived from modeling of Sr concentration and isotopes, as are the rates for the DSDP sites (Richter and Liang, 1993). Also shown are reaction rate data for bulk sediments from ODP Site 984A (+) (Maher et al., 2004), weathering rates from a soil chronosequence (*) (Taylor and Blum, 1995), and silicate weathering rates in granitic rocks (■ and □) (White et al., 1996, 2001).

minerals. Silicate weathering rates should be driven by the departure of the pore fluid chemical composition from equilibrium with the minerals. In soils and other clastic deposits, one can imagine that this departure is substantial. In the one siliciclastic deep-sea section studied thus far (Maher et al., 2004, 2006), there is evidence that the pore fluids are undersaturated by at least one order of magnitude relative to the primary silicate minerals. On the contrary, we contend that the pore fluid in carbonate sediments is essentially in equilibrium with calcite. The equilibrium cannot be demonstrated by measurements, because the pH and alkalinity measurements are too imprecise, but can be inferred from the Sr isotope data and the consideration of the reaction length for Ca. Nevertheless the rate of calcite dissolution, which in this case is mostly balanced by calcite precipitation, happens at a rate that is roughly consistent with the silicate dissolution rates as a function of age.

As a result of this analysis, we suggest that the departure from equilibrium (or the so-called "reaction affinity") has little effect on the reaction rate for the silicate mineral weathering process (Maher et al., 2006). For carbonate recrystallization, the reaction affinity is zero within the resolution of measurements and cannot be used to predict calcite recrystallization rates. The Sr isotopic data provide one of few available means to determine the rates of calcite recrystallization while the $^{234}U/^{238}U$ method (Maher et al., 2004, 2006) gives results similar to those obtained from soil studies for the age range of up to about 400,000 years. The U isotope method has not yet been applied to calcite recrystallization in deep-sea carbonate sections.

8. Conclusions

Estimates of the recrystallization rates in carbonate sediments from the Ontong Java Plateau from a steady-state perspective yield values between 0.042 Myr^{-1} in the upper part of the section and 0.005 Myr^{-1} in the lower part of the section. Numerical modeling of reaction and diffusion, constrained by measured Sr concentrations and isotopic composition, confirms these estimates of reaction rates and allows for further examination of pore fluid geochemistry.

Given the reaction rates calculated at 807A, the pore fluid Ca concentrations below 30–35 mbsf at 807A are due to equilibrium between pore fluids and calcite and are not determined by Ca sources within or below the sediment column. By recognizing equilibrium in the sediments, we are able to calculate the *in situ* pH in the pore fluids and compare them with the measured pH. We conclude that the measured pH at 807A is affected by sampling artifacts in all but a few cases. These unaffected cases agree quite well with our calculated pH.

By contrast with Ca, the pore fluid Mg concentrations at 807A are not controlled by equilibrium between calcite and fluid but instead are determined by the changing Mg concentration of seawater over time. We use our numerical model and estimates for important model parameters (of which K_{Mg} is not only the most critical but also the least constrained) to produce a record of the seawater Mg concentration over the past 35 million years. This record suggests that seawater Mg has risen rapidly over the past 10 million years (from about 35 mmol at 10 Ma to the present value of 52 mmol) rather than gradually over 40–60 Ma. Our global seawater Mg record agrees reasonably well with the few evaporite fluid inclusion data that cover this time period. We suggest that the recent rise in seawater Mg over the past 10 million years is controlled primarily by weathering inputs, driven by mountain building and climate changes, and not a decrease in Mg-removal processes such as hydrothermal weathering.

Finally, the relationship between reaction rate and age in silicates and carbonates is strikingly similar, leading to the conclusion that reaction affinity may not be as impor-

tant in determining low-temperature reaction rates as generally assumed. This suggestion is based on the surprisingly small difference in reaction rate between geologic materials of similar ages but vastly different chemical environment (far-from vs. near-equilibrium conditions). The influence of reaction affinity on the actual geologic reaction rates can be further investigated by applying various tools to the determination of reaction rates in natural systems. Thus far, two independent systems (Sr and U) have been used to constrain reaction rates in carbonate- and silicate-dominated sediments, respectively. The continued application of both methods should lead to a greater understanding of weathering over time and the role of reaction affinity in determining reaction rates. Most critical are measurements of systems younger than a few million years, to which pore fluid Sr measurements are not sensitive enough to measure weathering and recrystallization rates in sediments. However U, and possibly Ca, isotopes may be quite useful for studying inorganic diagenetic processes and reaction rates in Quaternary sediments.

Acknowledgments

The authors to thank F.M. Richter, Y. Liang, and J.M. Gieskes for their thorough and helpful reviews of the manuscript. This research was supported by the Director, Office of Science, Basic Energy Sciences, Chemical Sciences, Geosciences and Biosciences Division of the U.S. Department of Energy under Contract No. DE-AC02-05CH11231. Technical support was provided by Tom Owens. MSF was supported by a NASA Earth System Science Graduate Student Fellowship.

Associate editor: Robert H. Byrne

References

Baker, P.A., 1986. Pore-water chemistry of carbonate-rich sediments, Lord Howe Rise, Southwest Pacific Ocean. In: Kennett, J.P., von der Borch, C.C., Baker, P.A., et al. (Eds.), *Init. Repts. DSDP*, vol. 90. U.S. Govt Printing Office, pp. 1249–1256.

Baker, P.A., Stout, P.M., Kastner, M., Elderfield, H., 1991. Large-scale lateral advection of seawater through oceanic-crust in the central equatorial Pacific. *Earth Planet. Sci. Lett.* **105** (4), 522–533.

Berger, W.H., Kroenke, L.W., Mayer, L.A., et al., 1991. Ontong Java Plateau, Leg 130: synopsis of major drilling results. In: Kroenke, L.W., Berger, W.H., Janecek, T.R., et al. (Eds.), *Proc. ODP. Init. Reports*, vol. 130. Ocean Drilling Program, pp. 497–537.

Berner, R.A., 1980. *Early Diagenesis: A Theoretical Approach*. Princeton University Press, Princeton, NJ.

Berner, R.A., 2004. A model for calcium, magnesium and sulfate in seawater over Phanerozoic time. *Am. J. Sci.* **304** (5), 438–453.

Boudreau, B.P., 1997. *Diagenetic Models and Their Implementation: Modelling Transport and Reactions in Aquatic Sediments*. Springer, Berlin, New York.

Bralower, T.J., Premoli-Silva, I., Malone, M.J., et al., 2002. In: May, K.L. (Ed.), *Proceedings of the Ocean Drilling Program, Part A: Initial Reports*, vol. 198. Texas A&M University, Ocean Drilling Program.

Capo, R.C., DePaolo, D.J., 1990. Seawater strontium isotopic variations from 2.5 million years ago to the present. *Science* **249** (4964), 51–55.

Delaney, M.L., Linn, L.J., 1993. Interstitial water and bulk calcite chemisty, Leg 130, and calcite recrystallization. In: Berger, W.H., Kroenke, L.W., Janecek, T.R., et al. (Eds.), *Proc. ODP. Sci. Results*, vol. 130. Ocean Drilling Program, pp. 561–572.

De La Rocha, C.L., DePaolo, D.J., 2000. Isotopic evidence for variations in the marine calcium cycle over the cenozoic. *Science* **289** (5482), 1176–1178.

DePaolo, D.J., 1986. Detailed record of the Neogene Sr isotopic evolution of seawater from DSDP Site 590B. *Geology* **14** (2), 103–106.

DePaolo, D.J., 2004. Calcium isotopic variations produced by biological, kinetic, radiogenic and nucleosynthetic processes. In: Johnson, C.M., Beard, B.L., Albarede, F. (Eds.), *Geochemistry of non-traditional stable isotopes*, vol. 55. Mineralogical Society of America; Geochemical Society, pp. 255–285.

DePaolo, D.J., Finger, K.L., 1991. High-resolution strontium-isotope stratigraphy and biostratigraphy of the Miocene-Monterey-Formation, central California. *Geol. Soc. Am. Bull.* **103** (1), 112–124.

DePaolo, D.J., Getty, S.R., 1996. Models of isotopic exchange in reactive fluid-rock systems: implications for geochronology in metamorphic rock. *Geochim. Cosmochim. Acta* **60** (20), 3933–3947.

DePaolo, D.J., Ingram, B.L., 1985. High-resolution stratigraphy with strontium isotopes. *Science* **227** (4689), 938–941.

Dickson, A.G., 1990. Standard potential of the reaction: $AgCl(s) + 1/2H_2(g) = Ag(s) + HCl(aq)$ and the standard acidity constant of the ion HSO_4^- in synthetic sea-water from 273.15 to 318.15 K. *J. Chem. Thermodyn.* **22** (2), 113–127.

Fantle, M.S., DePaolo, D.J., 2005. Variations in the marine Ca cycle over the past 20 million years. *Earth Planet. Sci. Lett.* **237** (1-2), 102–117.

Gieskes, J.M., Lawrence, J.R., 1981. Alteration of volcanic matter in deep sea sediments: evidence from the chemical composition of interstitial waters from deep sea drilling cores. *Geochim. Cosmochim. Acta* **45** (10), 1687–1703.

Gieskes, J.M., Gamo, T., Brumsack, H., 1991. Chemical methods for interstitial water analysis aboard JOIDES resolution. Technical Note, pp. 1–60. Texas A&M University, College Station.

Gussone, N., Eisenhauer, A., Heuser, A., et al., 2003. Model for kinetic effects on calcium isotope fractionation (δ^{44}Ca) in inorganic aragonite and cultured planktonic foraminifera. *Geochim. Cosmochim. Acta* **67** (7), 1375–1382.

Hayes, W.W., Sloan, J.L., Wold, C.N., 1988. Mass age distribution and composition of sediments on the ocean-floor and the global rate of sediment subduction. *J. Geophys. Res.—Solid* **93** (B12), 14933–14940.

Hess, J., Bender, M.L., Schilling, J.G., 1986. Evolution of the ratio of Sr-87 to Sr-86 in seawater from Cretaceous to present. *Science* **231** (4741), 979–984.

Horita, J., Zimmermann, H., Holland, H.D., 2002. Chemical evolution of seawater during the Phanerozoic: implications from the record of marine evaporites. *Geochim. Cosmochim. Acta* **66** (21), 3733–3756.

Huang, Y., Fairchild, I.J., 2001. Partitioning of Sr^{2+} and Mg^{2+} into calcite under karst-analogue experimental conditions. *Geochim. Cosmochim. Acta* **65** (1), 47–62.

Johnson, J.W., Oelkers, E.H., Helgeson, H.C., 1992. SUPCRT92—a software package for calculating the standard molal thermodynamic properties of minerals, gases, aqueous species, and reactions from 1-bar to 5000-bar and 0 to 1000 °C. *Comput. Geosci.* **18** (7), 899–947.

Katz, A., 1973. Interaction of magnesium with calcite during crystal-growth at 25 °C and one atmosphere. *Geochim. Cosmochim. Acta* **37** (6), 1563–1586.

Katz, A., Sass, E., Starinsky, A., Holland, H.D., 1972. Strontium behavior in aragonite-calcite transformation—experimental study at 40–98 degrees C. *Geochim. Cosmochim. Acta* **36** (4), 481–496.

Krissek, L.A., Janecek, T.R., 1993. Eolian deposition on the Ontong Java Plateau since the Oligocene: unmixing a record of multiple dust sources. In: W.H. Berger, L.W. Kroenke, T.R. Janecek, et al. (Eds.), *Proc. ODP. Sci. Results*, vol. 130. Ocean Drilling Program, pp. 369–493.

Kroenke, L.W., Berger, W.H., Janecek, T.R., et al., 1991a. Explanatory notes. In: Kroenke, L.W., Berger, W.H., Janecek, T.R., et al. (Eds.),

Proc. ODP. Initial Reports, vol. 130. Ocean Drilling Program, pp. 15–43.

Kroenke, L.W., Berger, W.H., Janecek, T.R., et al., 1991b. Site 807. In: Kroenke, L.W., Berger, W.H., Janecek, T.R., et al. (Eds.), *Proc. ODP. Initial Reports*, vol. 130. Ocean Drilling Program, pp. 369–493.

Lasaga, A.C., 1998. *Kinetic Theory in the Earth Sciences*. Princeton University Press, Princeton, NJ.

Lemarchand, D., Wasserburg, G.T., Papanastassiou, D.A., 2004. Rate-controlled calcium isotope fractionation in synthetic calcite. *Geochim. Cosmochim. Acta* **68** (22), 4665–4678.

Lowenstein, T.K., Timofeeff, M.N., Brennan, S.T., Hardie, L.A., Demicco, R.V., 2001. Oscillations in Phanerozoic seawater chemistry: evidence from fluid inclusions. *Science* **294** (5544), 1086–1088.

Maher, K., DePaolo, D.J., Conrad, M.E., Serne, R.J., 2003. Vadose zone infiltration rate at Hanford, Washington, inferred from Sr isotope measurements. *Water Resour. Res.* **39** (8), 1204. doi:10.1029/2002WR001174.

Maher, K., DePaolo, D.J., Lin, J.C.F., 2004. Rates of silicate dissolution in deep-sea sediment: in situ measurement using U-234/U-238 of pore fluids. *Geochim. Cosmochim. Acta* **68** (22), 4629–4648.

Maher, K., Steefel, C.I., DePaolo, D.J., Viani, B.E., 2006. The mineral dissolution rate conundrum: insights from reactive transport modeling of U isotopes and pore fluid chemistry in marine sediments. *Geochim. Cosmochim. Acta* **70** (2), 337–363.

Mahoney, J.J., Storey, M., Duncan, R.A., Spencer, K.J., Pringle, M., 1993. Geochemistry and geochronology of Leg 130 basement lavas: nature and origin of the Ontong Java Plateau. In: Berger, W.H., Kroenke, L.W., Janecek, T.R., et al. (Eds.), *Proc. ODP. Sci. Results*, vol. 130. Ocean Drilling Program, pp. 3–22.

McDuff, R.E., Gieskes, J.M., 1976. Calcium and magnesium profiles in DSDP interstitial waters—diffusion or reaction? *Earth Planet. Sci. Lett.* **33** (1), 1–10.

Millero, F.J., 1982. The effect of pressure on the solubility of minerals in water and sea-water. *Geochim. Cosmochim. Acta* **46** (1), 11–22.

Millero, F.J., 1995. Thermodynamics of the carbon-dioxide system in the oceans. *Geochim. Cosmochim. Acta* **59** (4), 661–677.

Millero, F.J., 1996. *Chemical Oceanography*. CRC Press, Boca Raton.

Millero, F.J., 2001. *The Physical Chemistry of Natural Waters*. Wiley-Interscience, New York.

Mitterer, R.M., Malone, M.J., Goodfriend, G.A., Swart, P.K., Wortmann, U.G., Logan, G.A., Feary, D.A., Hine, A.C., 2001. Co-generation of hydrogen sulfide and methane in marine carbonate sediments. *Geophys. Res. Lett.* **28**, 3931–3934.

Molnar, P., 2004. Late Cenozoic increase in accumulation rates of terrestrial sediments: how might climate change have affected erosion rates? *Ann. Rev. Earth Planet Sci.* **32**, 67–89.

Morse, J.W., 2002. Sedimentary geochemistry of the carbonate and sulphide systems and their potential influence on toxic metal bioavailability. In: Gianguzza, A., Pelizzetti, E., Sammartano, S. (Eds.), *Chemistry of Marine Water and Sediments*. Springer, pp. 165–189.

Mucci, A., Morse, J.W., 1983. The incorporation of Mg^{2+} and Sr^{2+} into calcite overgrowths: Influences of growth-rate and solution composition. *Geochim. Cosmochim. Acta* **47** (2), 217–233.

Oomori, T., Kaneshima, H., Maezato, Y., Kitano, Y., 1987. Distribution coefficient of Mg^{2+} ions between calcite and solution at 10–50 °C. *Mar. Chem.* **20** (4), 327–336.

Phillips, O.M., 1991. *Flow and Reactions in Permeable Rocks*. Cambridge University Press, Cambridge [England].

Richter, F.M., 1993. Fluid flow in deep-sea carbonates: estimates based on porewater Sr. *Earth Planet. Sci. Lett.* **119**, 133–141.

Richter, F.M., 1996. Models for the coupled Sr-sulfate budget in deep-sea carbonates. *Earth Planet. Sci. Lett.* **141** (1–4), 199–211.

Richter, F.M., DePaolo, D.J., 1987. Numerical-models for diagenesis and the Neogene Sr isotopic evolution of seawater from DSDP Site 590B. *Earth Planet. Sci. Lett.* **83** (1–4), 27–38.

Richter, F.M., DePaolo, D.J., 1988. Diagenesis and Sr isotopic evolution of seawater using data from DSDP-590B and DSDP-575. *Earth Planet. Sci. Lett.* **90** (4), 382–394.

Richter, F.M., Liang, Y., 1993. The rate and consequences of Sr diagenesis in deep-sea carbonates. *Earth Planet. Sci. Lett.* **117** (3–4), 553–565.

Rudnicki, M.D., Elderfield, H., Mottl, M.J., 2001a. Pore fluid advection and reaction in sediments of the eastern flank, Juan de Fuca Ridge, 48 °N. *Earth Planet. Sci. Lett.* **187**, 173–189.

Rudnicki, M.D., Wilson, P.A., Anderson, W.T., 2001b. Numerical models of diagenesis, sediment properties, and pore fluid chemistry on a paleoceanographic transect: Blake Nose, Ocean Drilling Program Leg 171B. *Paleoceanography* **16** (6), 563–575.

Rushdi, A.I., McManus, J., Collier, R.W., 2000. Marine barite and celestite saturation in seawater. *Mar. Chem.* **69** (1–2), 19–31.

Schmitt, A.D., Bracke, G., Stille, P., Kiefel, B., 2001. The calcium isotope composition of modern seawater determined by thermal ionisation mass spectrometry. *Geostandard Newslett.* **25** (2-3), 267–275.

Schrag, D.P., Depaolo, D.J., Richter, F.M., 1995. Reconstructing past sea-surface temperatures—correcting for diagenesis of bulk marine carbonate. *Geochim. Cosmochim. Acta* **59** (11), 2265–2278.

Spinelli, G.A., Giambolvo, E.R., Fisher, A.T., 2004. Sediment permeability, distribution, and influence on fluxes in oceanic basement. In: Davis, E.E., Elderfield, H. (Eds.), *Hydrogeology of the Oceanic Lithosphere*. Cambridge University Press, pp. 151–188.

Steefel, C., 2001. *Software for Modeling Multicomponent, Multidimensional Reactive Transport*. Lawrence Livermore Laboratory.

Taylor, A., Blum, J.D., 1995. Relation between soil age and silicate weathering rates determined from the chemical evolution of a glacial chronosequence. *Geology* **23** (11), 979–982.

White, A.F., Brantley, S.L., 2003. The effect of time on the weathering of silicate minerals: why do weathering rates differ in the laboratory and field? *Chem. Geol.* **202** (3-4), 479–506.

White, A.F., Blum, A.E., Schulz, M.S., Bullen, T.D., Harden, J.W., Peterson, M.L., 1996. Chemical weathering rates of a soil chronosequence on granitic alluvium .1. Quantification of mineralogical and surface area changes and calculation of primary silicate reaction rates. *Geochim. Cosmochim. Acta* **60** (14), 2533–2550.

White, A.F., Bullen, T.D., Schulz, M.S., Blum, A.E., Huntington, T.G., Peters, N.E., 2001. Differential rates of feldspar weathering in granitic regoliths. *Geochim. Cosmochim. Acta* **65** (6), 847–869.

Zachos, J., Pagani, M., Sloan, L., Thomas, E., Billups, K., 2001. Trends, rhythms, and aberrations in global climate 65 Ma to present. *Science* **292** (5517), 686–693.

Zimmermann, H., 2000. Tertiary seawater chemistry—implications from primary fluid inclusions in marine halite. *Am. J. Sci.* **300** (10), 723–767.